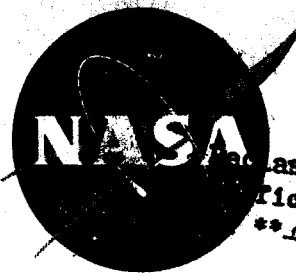


NASA TM X-11



Declassified by authority of NASA
Classification Change Notices No. 50
** 2/16/66

TECHNICAL MEMORANDUM

X-11

DECLASSIFIED- AUTHORITY
US: 663 DROBKA TO LEBOW
MEMO DATED 2/1/66
1/10/66

AERODYNAMIC CHARACTERISTICS IN PITCH, INCLUDING EFFECTS
OF HORIZONTAL-TAIL NEGATIVE DIHEDRAL ANGLE, OF A
0.048-SCALE MODEL OF A HORIZONTAL-ATTITUDE
VTOL AIRPLANE AT TRANSONIC SPEEDS

By Walter B. Olstad

Langley Research Center
Langley Field, Va

FACILITY FORM 602

N66-20899
(ACCESSION NUMBER)

55
(PAGES)

(THRU)

1
(CODE)

(NASA CR OR TMX CR AD NUMBER)

01
(CATEGORY)

GPO PRICE \$ _____

CFSTI PRICE(S) \$ _____

Hard copy (HC) \$ 3.00

Microfiche (MF) \$ 2.00

ff 653 July 65

NATIONAL AERONAUTICS AND SPACE ADMINISTRATION
WASHINGTON
October 1960

REF ID: A60000

NATIONAL AERONAUTICS AND SPACE ADMINISTRATION

TECHNICAL MEMORANDUM X-11

AERODYNAMIC CHARACTERISTICS IN PITCH, INCLUDING EFFECTS
OF HORIZONTAL-TAIL NEGATIVE DIHEDRAL ANGLE, OF A
0.048-SCALE MODEL OF A HORIZONTAL-ATTITUDE
VTOL AIRPLANE AT TRANSONIC SPEEDS*

By Walter B. Olstad

SUMMARY

20899

An investigation was made of the aerodynamic characteristics in pitch of a 0.048-scale model of a horizontal-attitude vertical-take-off-and-landing (VTOL) airplane at Mach numbers from 0.60 to 1.20 and at angles of attack up to 25° . The effects of horizontal-tail negative dihedral and a modification to the fuselage indentation were also studied.

The results indicated that the configuration with the 0° dihedral horizontal tail was statically unstable at zero lift for test Mach numbers from 0.60 to 1.05. Decreasing the horizontal-tail dihedral angle increased the static stability of the model. The configuration with the -30° dihedral horizontal tail was statically stable throughout the Mach number range of the investigation although it approached a condition of neutral stability at a Mach number of 0.90. The effectiveness of horizontal-tail negative dihedral in increasing the static stability of the model was due mainly to the effective lowering of the horizontal tail. The modification to the fuselage indentation of the model permitted an increase in useful volume without incurring a large drag penalty.

quisha

INTRODUCTION **Declassified by authority of NASA**
Classification Change Notices No. 50
Dated ** 2/16/66

The model tested is a horizontal-attitude supersonic airplane with vertical take-off and landing capabilities. Vertical flight is achieved by rotating the wing-tip engine nacelles so that they are aligned with the vertical. The jets from the two engines mounted in the rear of the

*Title, Unclassified.

C [REDACTED]

fuselage are directed downward by means of cascades. Two engines mounted forward in the fuselage are used only for vertical flight. In forward flight, the wing-tip nacelles are aligned with the wing-chord plane and the jets from the engines mounted in the rear of the fuselage are directed rearward.

An investigation of the aerodynamic characteristics of this VTOL airplane has been conducted at transonic speeds in the Langley 8-foot transonic pressure tunnel. This configuration was tested at Mach numbers ranging from 0.60 to 1.20 and at angles of attack up to 25° . The effects of horizontal-tail negative dihedral angle were investigated in addition to the effects of a change in fuselage shape. The average test Reynolds number based on the wing mean aerodynamic chord varied from 1.42×10^6 to 1.90×10^6 over the Mach number range of the investigation.

SYMBOLS

\bar{c}_t	tail mean aerodynamic chord, in.
\bar{c}_w	wing mean aerodynamic chord, in.
C_D	drag coefficient, $\frac{\text{Drag}}{qS_w}$
$C_{D,i}$	internal drag coefficient
$C_{D,\min}$	minimum drag coefficient
$\frac{\partial C_D}{\partial C_L^2}$	drag due to lift factor, averaged from $C_L = 0$ to $C_L = 0.3$
ΔC_D	incremental drag coefficient due to speed brakes
C_L	lift coefficient, $\frac{\text{Lift}}{qS_w}$
$C_{L,\text{opt}}$	lift coefficient for maximum lift-drag ratio
$C_{L\alpha}$	lift-curve slope per degree, averaged from $\alpha = 0^\circ$ over linear portion of curve

- $(C_{L\alpha})_t$ lift-curve slope per degree of horizontal tail
- C_m pitching-moment coefficient, $\frac{\text{Pitching moment}}{qS_w\bar{c}_w}$
- $C_{m,t}$ pitching-moment coefficient contributed by horizontal tail
- $\frac{\partial C_m}{\partial C_L}$ static-longitudinal-stability parameter
- $C_{p,b}$ base pressure coefficient, $\frac{P_b - P_\infty}{q}$
- l distance from $0.25\bar{c}_t$ to airplane center of gravity, in.
- $(L/D)_{\max}$ maximum lift-drag ratio
- M free-stream Mach number
- p_b static pressure at model base, lb/sq ft
- p_∞ free-stream static pressure, lb/sq ft
- q free-stream dynamic pressure, lb/sq ft
- R Reynolds number based on wing mean aerodynamic chord
- S_t exposed tail area, sq ft
- S_w total wing area (measured between nacelle center lines), sq ft
- t_{\max} maximum wing section thickness
- $C_{v,t}$ tail volume coefficient, $\frac{l}{\bar{c}_w} \frac{S_t}{S_w}$
- w mass flow through model
- w_∞ mass flow through a free-stream tube of the same area as the inlet
- α angle of attack, deg



L
2
4
3

- ϵ effective downwash angle at horizontal tail, deg
- $\frac{\partial \epsilon}{\partial \alpha}$ rate of change of effective downwash angle at horizontal tail with angle of attack
- τ tail stability parameter

Model component designations:

- B_1 original fuselage L
- B_2 modified fuselage obtained by partially filling in the indentation of the original body 2
- F_1 small ventral fin 4
- F_2 large ventral fin 3
- H_0 horizontal tail with 0° dihedral angle
- H_{15} horizontal tail with -15° dihedral angle
- H_{30} horizontal tail with -30° dihedral angle
- N wing-tip engine nacelles
- V_1 small vertical tail
- W wing

APPARATUS AND TESTS

Tunnel

The tests were conducted in the Langley 8-foot transonic pressure tunnel which is a rectangular, slotted-throat, single-return tunnel designed to obtain aerodynamic data at transonic speeds while minimizing the effects of choking and blockage. During this investigation, the tunnel was operated at a stagnation pressure of approximately 1 atmosphere. The dewpoint of the tunnel air was controlled and was kept constant at approximately 0° F. The stagnation temperature of the tunnel was automatically controlled and was kept constant and uniform across the tunnel at 121° F. Control of both dewpoint and stagnation



temperature in this manner minimized humidity effects. Details of the test section have been presented in reference 1.

Model

Dimensional details of the 0.048-scale model of a horizontal-attitude VTOL airplane are presented in figure 1 and table I. Photographs of the model shown mounted in the Langley 8-foot transonic pressure tunnel are presented in figure 2.

The wing, which was mounted high on the fuselage, was unswept along the 50-percent-chord line. It had an aspect ratio of 2.42 and a taper ratio of 0.433. The streamwise airfoil section was a modified NACA 65A005. The modification consisted of straight-line fairing from the 60 percent chord to the blunt trailing edge. The thickness of this trailing edge was 30 percent of the maximum thickness of the local airfoil section.

The fuselage, which had a fineness ratio of 10.4, was designed according to the supersonic area-rule concept and was indented for the wing and nacelles in order to give a favorable area distribution at a design Mach number of 1.4. The indentation was modified during this investigation by adding some volume to the fuselage in the vicinity of the wing. The modification resulted in replacing approximately 25 percent of the volume removed by full indentation.

Two ram-type inlets with boundary-layer diverter plates were mounted on the sides of the fuselage beneath the wing. The air taken into these inlets was exhausted at the base of the model.

An engine nacelle was mounted on each wing tip. These nacelles were of fineness ratio 4.47. The fineness ratio was based on the total cross-sectional area of the nacelle, including that of the entering stream tube.

One vertical tail and two ventral fins were tested. All of these vertical surfaces were swept back along the quarter-chord line at approximately 50° . Three sets of all-movable horizontal tails varying in dihedral angle were investigated. The three dihedral angles were 0° , -15° , and -30° . The larger ventral fin was designed for use with the 0° horizontal tail; the smaller ventral fin was designed for use with the 15° horizontal tail; and the 30° horizontal tail was designed for use without a ventral fin. Details of these various tail arrangements are presented in figure 1(b).

Two speed brakes were also tested, one on the upper surface of the fuselage behind the vertical tail and one on the lower surface of



the fuselage behind the ventral fin. Details of the speed brakes are presented in figure 1(c).

Measurements and Accuracy

Model forces and moments were measured by a six-component internal strain-gage balance and converted to lift, drag, and pitching moment about the stability axes originating at a center-of-gravity location at 33 percent of the wing mean aerodynamic chord and 14.15 percent of the mean aerodynamic chord below the wing-chord plane. Accuracies of the coefficients are estimated to be within the following limits:

C_L	±0.02
C_D	±0.004
C_m	±0.01

L
2
4
3

The angles of attack were determined to within $\pm 0.15^\circ$ by a pendulum-type inclinometer located in the sting support and from a calibration of sting and balance deflection with respect to model load. Rakes of static- and total-pressure tubes located at the base of the fuselage and at the base of each nacelle were used to determine the internal drag coefficients and mass-flow ratios. The internal drag coefficients are estimated to be accurate to within ± 0.0005 . The accuracy of the mass-flow ratios is estimated to be within ± 0.02 . Base pressure coefficients were obtained from static-pressure orifices located at the base of the fuselage, at the base of each nacelle, and in the balance chamber. The accuracy of these base pressure coefficients is estimated to be ± 0.05 .

Tests

The model was tested at Mach numbers from 0.60 to 1.20 at angles of attack from approximately -2° to approximately 25° . During these tests the average test Reynolds number based on the wing mean aerodynamic chord varied from 1.42×10^6 to 1.90×10^6 . (See fig. 3.) The average test dynamic pressure was also included in figure 3.

For the tests with fixed transition, 0.10-inch transition strips were located at 10 percent of the chord on all aerodynamic surfaces and at 10 percent of the fuselage and nacelle lengths. The strips were obtained by spraying the surfaces with a commercial liquid plastic and blowing on grains of carborundum (approx. 0.012 inch in diameter) at an estimated density of 40 grains per inch.



Corrections

Subsonic boundary interference is minimized by the slotted test section, and no corrections for this interference have been applied. The effects of supersonic boundary-reflected disturbances were reduced by testing the model several inches from the tunnel center line. No corrections for sting interference have been applied. The drag data have been adjusted to an assumed condition of free-stream static pressure acting over the model base by the base pressure coefficients presented in figure 4. The drag data also have been corrected for internal drag by use of the internal drag coefficients presented in figure 5. (In order to facilitate presentation of the data, staggered scales have been used in many of the figures and care should be taken in identifying the proper scale for each curve.) No sting-interference corrections have been applied.

RESULTS

Typical mass-flow ratios for the model are presented in figure 6 as a function of Mach number. The basic aerodynamic characteristics in pitch for the various complete-model configurations are presented in figures 7, 8, and 9. Pitching-moment data plotted as a function of lift coefficient for the model with the horizontal tail removed are presented in figure 10. These data were used to determine the pitching-moment coefficient contributed by the horizontal tail $C_{m,t}$. In figure 11, the lift coefficient is presented for the three horizontal-tail configurations with the wing removed at various Mach numbers. These data were used to determine the lift-curve slope of the horizontal tail $(C_{L\alpha})_t$.

A brief analysis of the longitudinal characteristics is presented in figures 12 to 18. The variation with angle of attack of the effective downwash angle at the horizontal tail shown in figure 14 was obtained from the expression

$$C_{m,t} = (C_{L\alpha})_t C_{v,t} (\alpha - \epsilon)$$

The tail stability parameter (fig. 16) was computed from the equation given in reference 2:

$$\tau = \frac{\partial C_{m,t}}{\partial \alpha} \frac{1}{C_{L\alpha} C_{v,t}}$$

CONFIDENTIAL

The variation with Mach number of the incremental drag coefficient due to speed brakes is shown in figure 19.

DISCUSSION OF RESULTS

Lift and Pitching-Moment Characteristics

Lift characteristics.- The lift curves for the various model configurations tested were generally linear for lift coefficients up to 0.6 throughout the Mach number range. (See figs. 7, 8(a), and 9(a).) The lift-curve slope of the model with the 0° dihedral horizontal tail varied from 0.081 at a Mach number of 0.60 to 0.112 at a Mach number of 0.95 (fig. 12). As the horizontal-tail dihedral angle was reduced from 0° to -15°, the lift-curve slope of the model increased by approximately 2.5 percent throughout the Mach number range. As the horizontal-tail dihedral angle was reduced from 0° to -30°, the lift-curve slope of the model increased by approximately 6 percent throughout the Mach number range.

Pitching-moment characteristics.- The pitching-moment coefficient curves for the various complete-model configurations (figs. 7, 8(b), and 9(b)) were generally nonlinear throughout the lift-coefficient range. A condition of extreme stability was reached at lift coefficients between 0.7 to 0.8. The value of the static-longitudinal-stability

parameter $\frac{\partial C_m}{\partial C_L}$ at zero lift for the model with 0° dihedral horizontal tail increased from about 0.03 at a Mach number of 0.60 to a peak value of 0.13 at a Mach number of 0.90 and then decreased to about -0.10 at a Mach number of 1.20 (fig. 13). The model with 0° dihedral horizontal tail became stable at zero lift at a Mach number 1.05. Decreasing the horizontal-tail dihedral angle from 0° to -15° decreased the static-longitudinal-stability parameter by approximately 0.025 to 0.075 throughout the Mach number range. However, this configuration was still unstable for all Mach numbers tested below 0.97. Decreasing the horizontal-tail dihedral angle from 0° to -30° decreased the static-longitudinal-stability parameter by 0.10 to 0.13 throughout the Mach number range. This configuration was stable at zero lift throughout the Mach number range although it approached a condition of neutral stability at a Mach number of 0.90. Figure 13 also shows that decreasing the horizontal-tail dihedral angle added stability to the model throughout the Mach number range for a lift coefficient of 0.4. At this lift coefficient only the model with the 0° dihedral horizontal tail exhibited any instability and that occurred in the immediate vicinity of a Mach number of 0.90.

CONFIDENTIAL

DECLASSIFIED

Effective downwash characteristics.- The variation of the effective downwash angle at the horizontal tail with angle of attack is presented in figure 14 for configurations with 0° , -15° , and -30° horizontal-tail dihedral angles. The downwash characteristics are different for the three tails because the tails vary in effective vertical location. The horizontal tail with the 0° dihedral angle is in the highest effective vertical location while the horizontal tail with the -30° dihedral angle is in the lowest effective vertical location.

L
2
4
3
The average rate of change of downwash angle with angle of attack for angles of attack from -2° to 4° is plotted as a function of angle of attack in figure 15. The effective downwash derivative $\partial\epsilon/\partial\alpha$ increased rapidly from a Mach number of 0.60 to a Mach number of 0.95 and then decreased rapidly through the transonic regime to a Mach number of 1.20 for all three horizontal-tail configurations. The effect of decreasing the horizontal-tail dihedral angle (lowering the effective vertical location) was to decrease the effective downwash derivative throughout the Mach number range.

Contribution of horizontal tail to stability.- Figure 16 shows the variation with angle of attack of the tail stability parameter τ for horizontal-tail dihedral angles of 0° , -15° , and -30° . The tail stability parameter generally became more negative, that is, the configuration became more stable, with increasing angle of attack for angles of attack up to about 12° . A decrease in horizontal-tail dihedral angle generally increased the stability of the model for angles of attack up to about 10° . This increase in stability with decrease in horizontal-tail dihedral angle was largely due to the decrease in effective downwash derivative. The effective downwash derivative is a function of the vertical position of the tail with respect to the wing but not of the tail geometry. Thus, it appears that the effectiveness of horizontal-tail dihedral angle in increasing the airplane stability is due mainly to the effective lowering of the horizontal tail.

Drag Characteristics

Minimum drag.- The effect on the minimum drag of a modification to the indentation of the model fuselage is shown in figure 17. The modification consisted of replacing approximately 25 percent of the volume removed by full indentation. At subsonic speeds, the minimum drag coefficient for the two configurations with transition fixed is about 0.041. This value is quite large because of the large amount of wetted area presented to the flow by the fuselage, nacelles, and aerodynamic surfaces. At Mach numbers above 0.9, the modification had only a minor effect on the minimum drag coefficient except in the neighborhood of $M = 1.05$ where the modification increased the minimum drag coefficient

by about 0.005. Thus, the modification permitted an increase in useful volume without incurring a large drag penalty.

Fixing transition (fig. 17) generally increased the minimum drag coefficient by 0.002 to 0.004 throughout the Mach number range. The effect of decreasing horizontal-tail dihedral angle on the minimum drag coefficient was negligible and has not been presented.

Drag at lifting conditions.- The drag-due-to-lift factor $\frac{\partial C_D}{\partial C_L^2}$

averaged over a lift-coefficient range from 0 to 0.3 increased steadily from a value of about 0.145 at a Mach number of 0.60 to 0.195 at a Mach number of 1.20. (See fig. 17.) The effects of the modification to the body and of transition were negligible and are not presented for the sake of clarity. The effect of changing the horizontal-tail dihedral angle on the drag-due-to-lift factor was also negligible and has not been included in the figure. Since the changes in horizontal-tail dihedral angle had no noticeable effect upon the drag characteristics of the model, all of the following discussion which relates specifically to the configuration with the 0° dihedral horizontal tail also applies to the configurations with -15° and -30° dihedral horizontal tails.

The maximum lift-drag ratio for the model was nearly constant at a value of 6.4 for the Mach number range from 0.60 to 0.90. (See fig. 18.) The maximum lift-drag ratio then decreased sharply to a value of about 4.7 at a Mach number of 1.00 and began decreasing more slowly to a value of 3.9 at a Mach number of 1.20. These relatively low values of maximum lift-drag ratio are caused in part by the large friction drag discussed previously. At full-scale Reynolds numbers, it is expected that the friction-drag coefficient would not be so high and the maximum lift-drag ratio would be increased. In order to illustrate this effect, the friction-drag coefficient at several Mach numbers was adjusted to a Reynolds number of 20×10^6 (with fully developed turbulent flow assumed). This Reynolds number is approximately that which would be obtained on the full-scale airplane in level flight at $C_{L_{opt}}$. It has been assumed that the surface roughness of the full-scale airplane is comparable with that of the model. The resulting lift-drag ratios are indicated in figure 18.

The lift coefficient for maximum lift-drag ratio increased from approximately 0.41 at a Mach number of 0.60 to 0.72 at a Mach number of 1.05. Values of $C_{L_{opt}}$ adjusted to full-scale Reynolds number are presented in figure 18.

DECLASSIFIED

11

Effect of speed brakes.- Speed brakes were added to the configuration with the 0° horizontal tail in the locations indicated in figure 1(c). Figure 19 indicates that the addition of these speed brakes produced an incremental drag coefficient of about 0.061 to 0.065 at subsonic speeds, which decreased to approximately 0.055 at Mach numbers of 1.13 and above.

CONCLUSIONS

L
2
4
3
An investigation of the aerodynamic characteristics in pitch, including the effects of horizontal-tail negative dihedral angle, of a 0.048-scale model of a horizontal-attitude VTOL airplane at transonic speeds has led to the following conclusions:

1. The model with a 0° dihedral horizontal tail was statically unstable at zero lift for test Mach numbers from 0.60 to 1.05. Decreasing the horizontal-tail dihedral angle increased the static stability of the model. The configuration with the -30° dihedral horizontal tail was statically stable throughout the Mach number range although it approached a condition of neutral stability at a Mach number of 0.90.

2. The effectiveness of horizontal-tail negative dihedral in increasing the static stability of the model was due mainly to the effective lowering of the horizontal tail.

3. A modification to the fuselage of the model which consisted of replacing approximately 25 percent of the volume removed by full indentation permitted an increase in useful volume without incurring a large drag penalty.

Langley Research Center,
National Aeronautics and Space Administration,
Langley Field, Va., February 17, 1959.

03712201030

REFERENCES

1. Mugler, John P., Jr.: Transonic Wind-Tunnel Investigation of the Aerodynamic Loading Characteristics of a 60° Delta Wing in the Presence of a Body With and Without Indentation. NACA RM L55G11, 1955.
2. Foster, Gerald V., and Griner, Roland F.: Low-Speed Longitudinal and Wake Air-Flow Characteristics at a Reynolds Number of 5.5×10^6 of a Circular-Arc 52° Sweptback Wing With a Fuselage and a Horizontal Tail at Various Vertical Positions. NACA RM L51C30, 1951.

L
2
4
3

CONFIDENTIAL

TABLE I.- DIMENSIONS OF A 0.048-SCALE MODEL OF
THE HORIZONTAL-ATTITUDE VTOL AIRPLANE

Center-of gravity location:

Longitudinal (station 16.644 in.)	0.33 \bar{c}_w
Vertical	0.768 in. below \bar{c}_w

Wing:

Airfoil section	Modified 65A005 (trailing-edge thickness, $0.3t_{max}$)
Total area (measured between nacelle center lines), sq ft	0.447
Span (measured between nacelle center lines), in.	12.456
Mean aerodynamic chord, \bar{c}_w , in.	5.424
Aspect ratio	2.42
Taper ratio	0.433
Sweepback of quarter-chord line, deg	9.3
Incidence, deg	0
Dihedral, deg	0
Distance of \bar{c}_w above body reference line, in.	1.056

Horizontal tails:

	H_0	H_{15}	H_{30}
Airfoil section	NACA 65A004	NACA 65A004	NACA 65A004
Exposed area, sq ft	0.1051	0.1090	0.1212
Exposed span, in.	6.528	6.528	6.528
Mean aerodynamic chord of exposed tail, \bar{c}_t , in.	2.405	2.496	2.772
Exposed aspect ratio	2.81	2.71	2.44
Exposed taper ratio	0.496	0.496	0.497
Sweep of quarter-chord line, deg	29.6	29.6	29.6
Incidence, deg	0	0	0
Dihedral, deg	0	-15	-30
Tail length, in.	12.168	12.300	12.370
Distance of \bar{c}_t below body reference line, in.	0.163	1.220	1.836

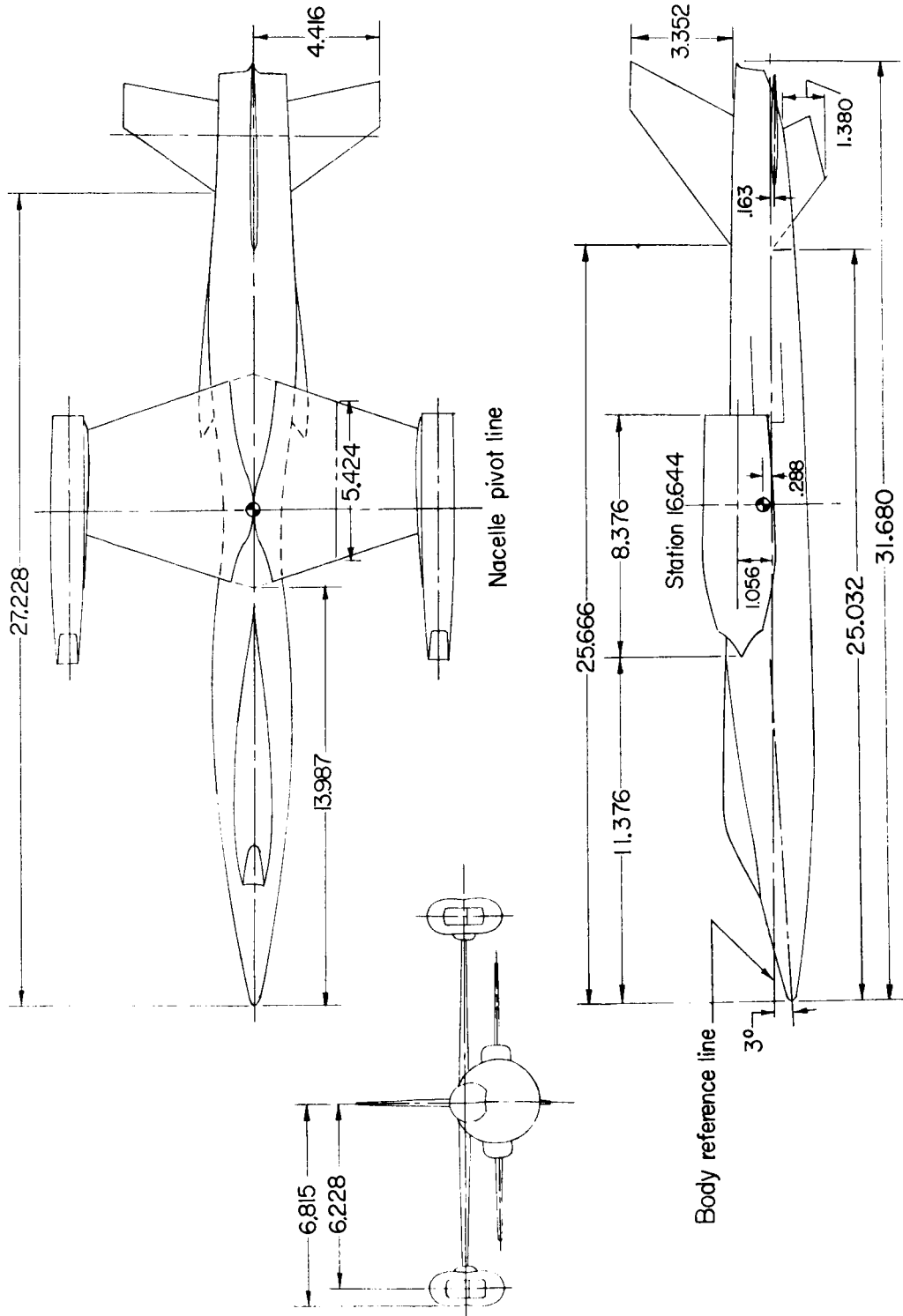
Vertical tail:

Airfoil section	NACA 65A004
Exposed area, sq ft	0.0638
Exposed span, in.	3.264
Exposed aspect ratio	1.16
Exposed taper ratio	0.408
Sweepback of quarter-chord line, deg	47.55

Ventral fins:

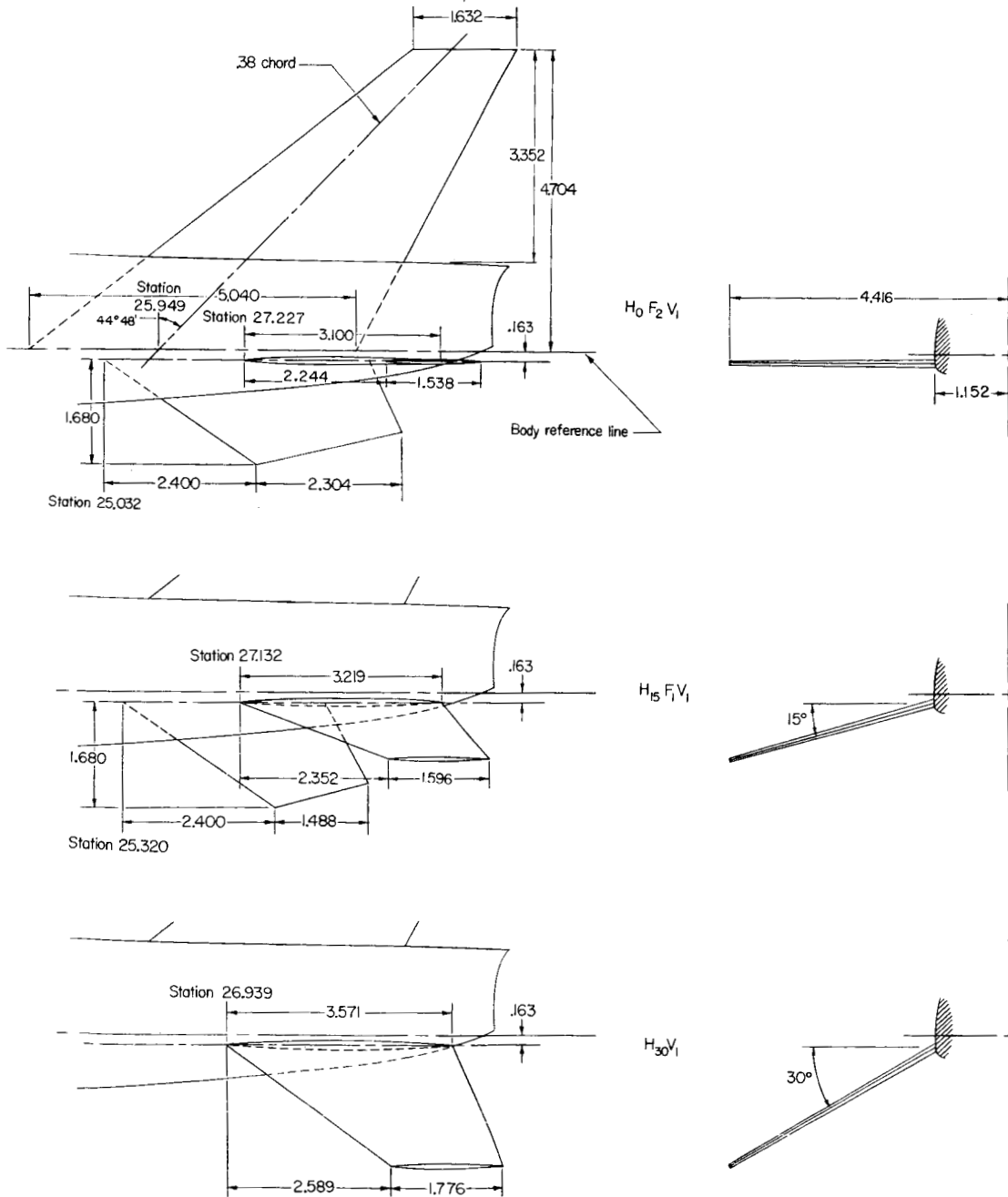
	F_1	F_2
Airfoil section	NACA 65A004	NACA 65A004
Total area, sq ft	0.0264	0.0342
Total span, in.	1.680	1.680
Aspect ratio	0.656	0.357
Taper ratio	0.463	0.620
Sweepback of quarter-chord line, deg	47.78	49.00

L-243



(a) Complete model.

Figure 1.- Drawing of a 0.048-scale model of the horizontal-attitude VTOL airplane. All dimensions are in inches unless otherwise noted.

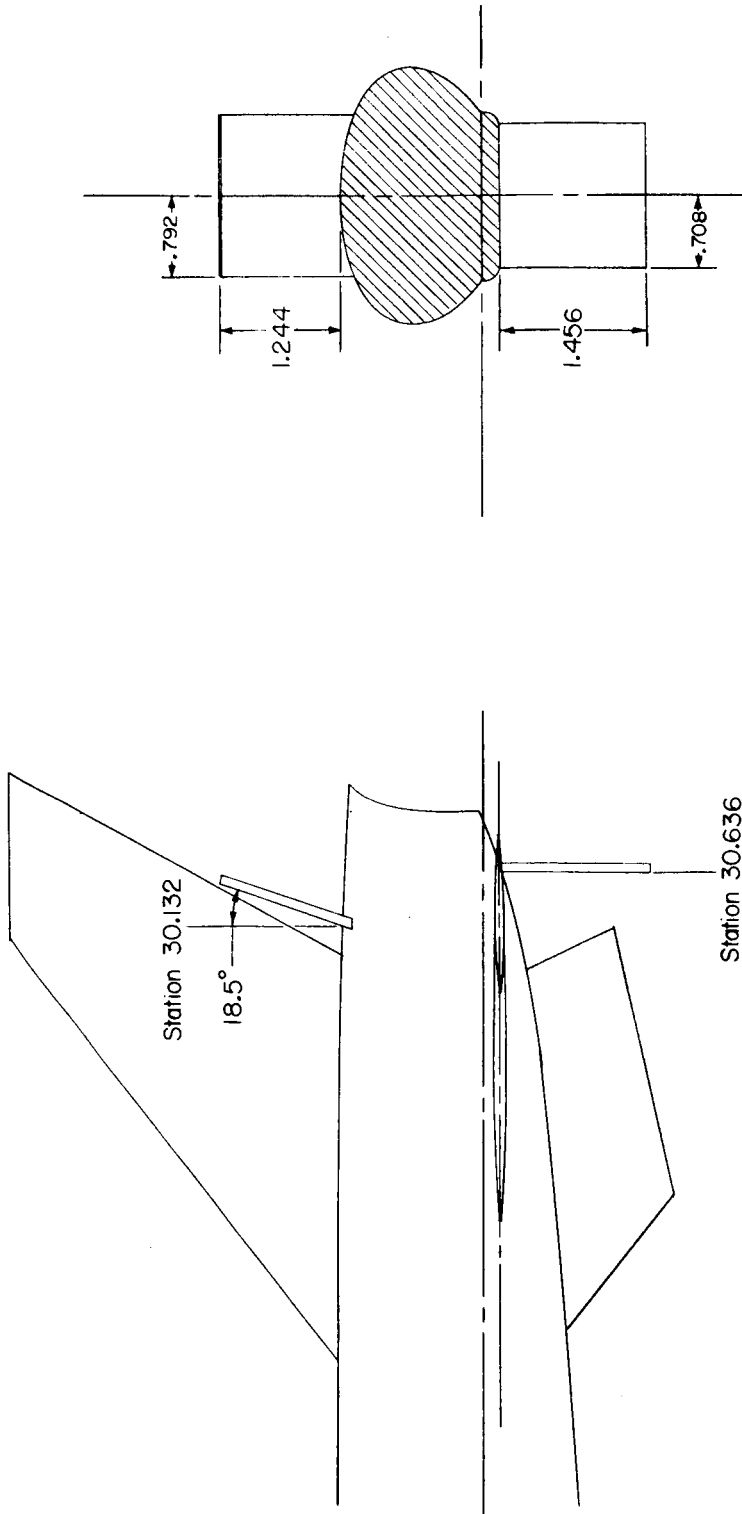


(b) Details of tail arrangements.

Figure 1.- Continued.



I-243



(c) Details of speed brakes.

Figure 1.- Concluded.

L-243

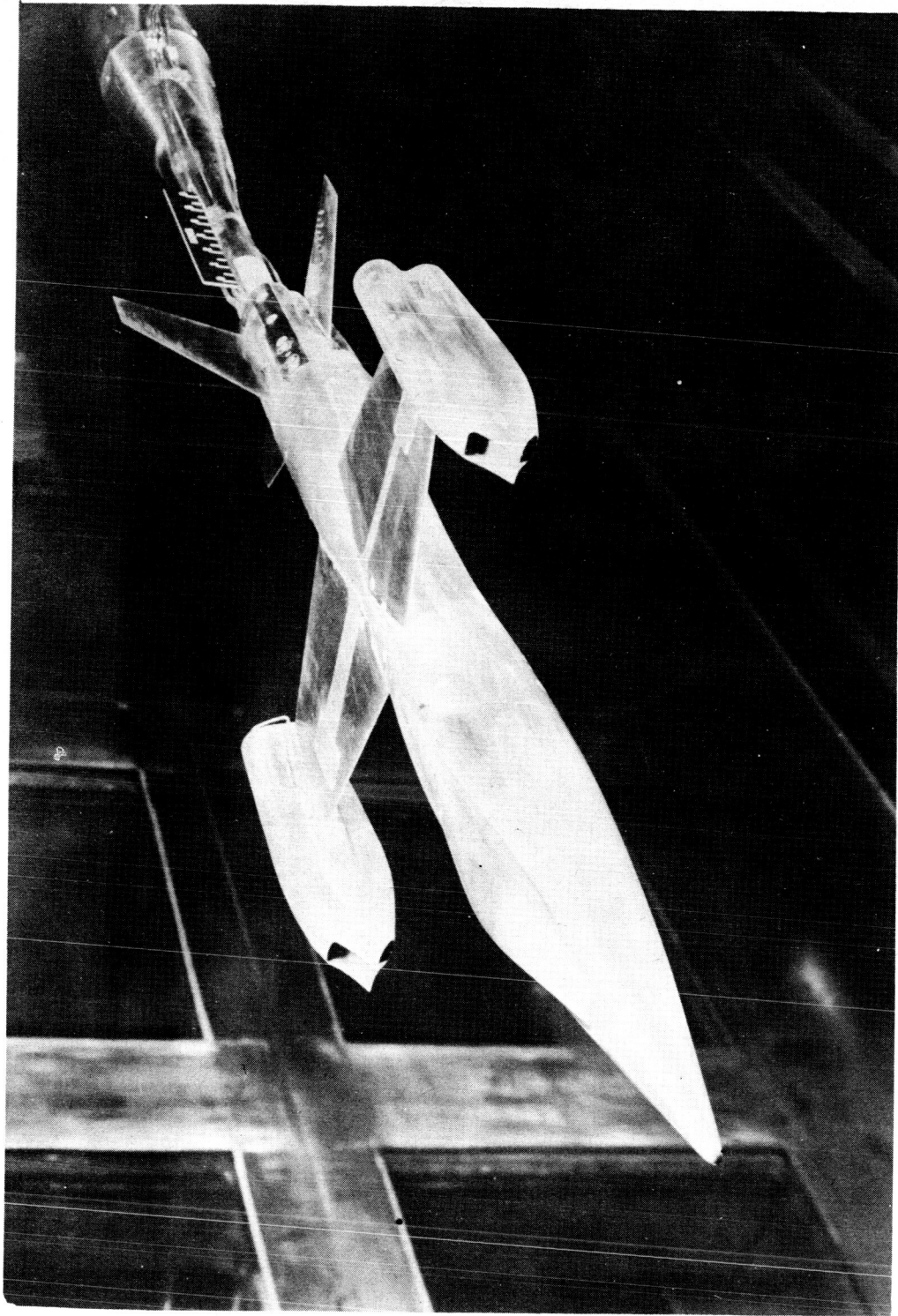


Figure 2.- Model configuration WB₁NH₀F₂V₁ mounted in the Langley 8-foot transonic pressure tunnel.



03 70 24 10 03

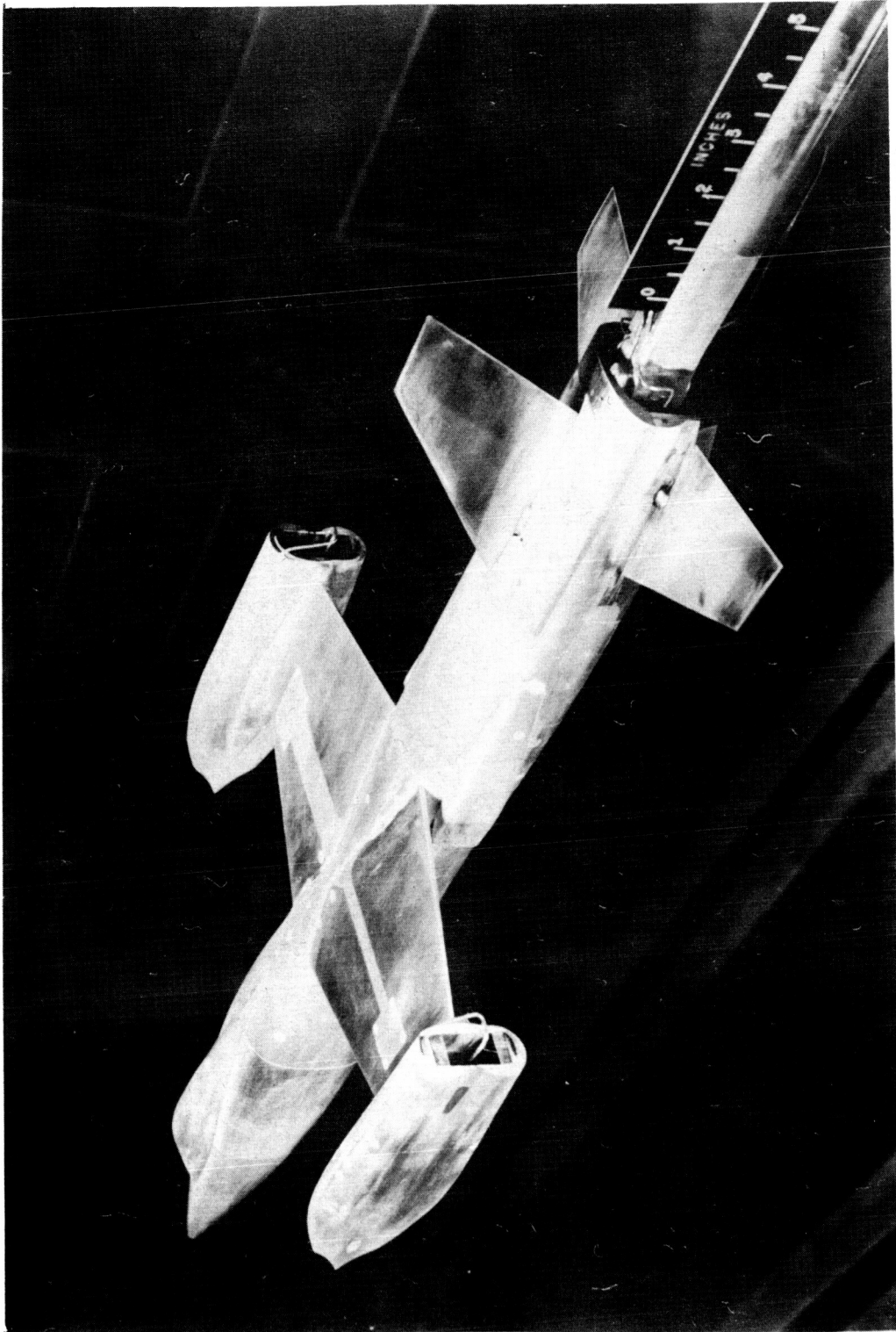
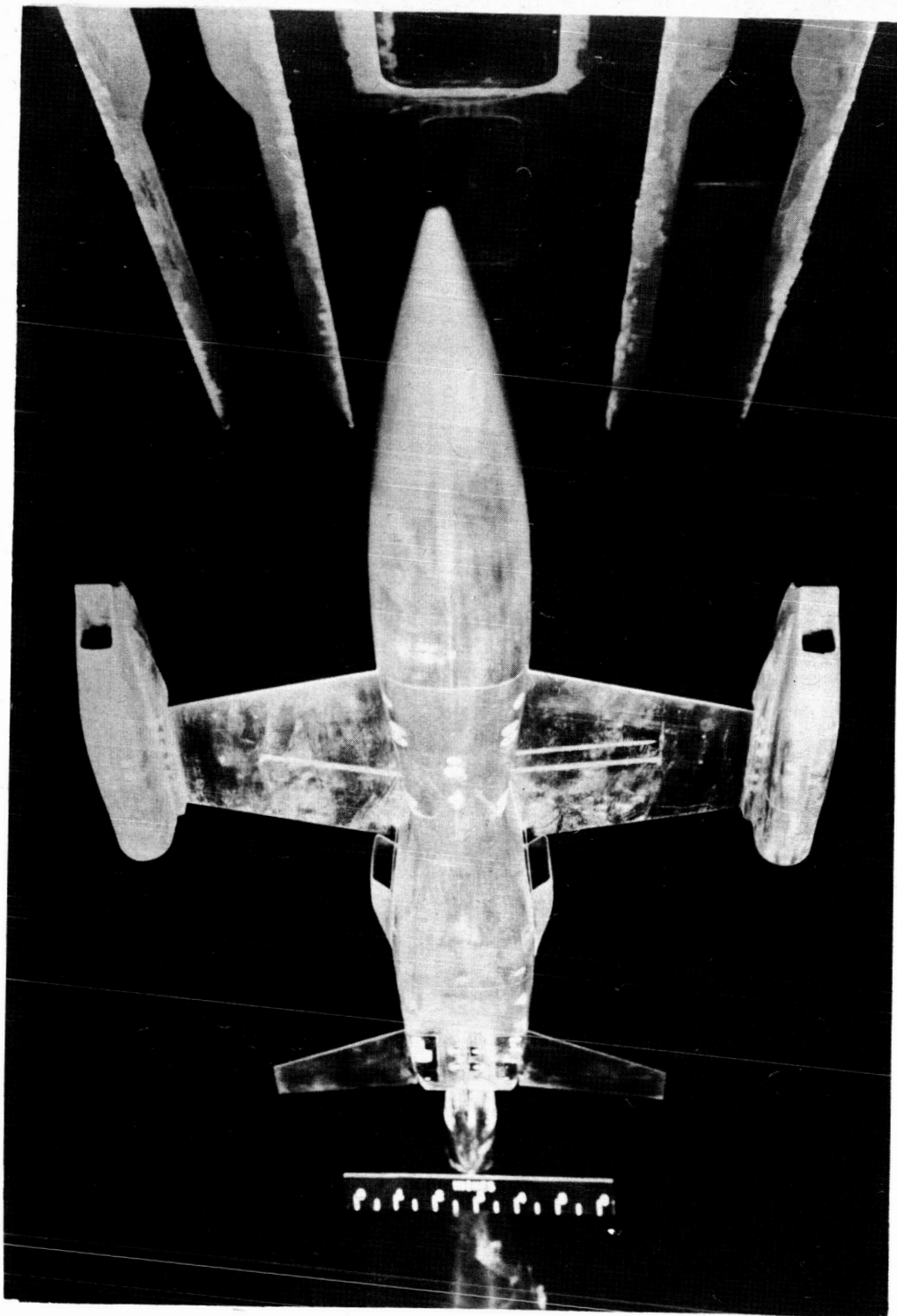


Figure 2.- Continued. L-58-1125



L-243

Figure 2.- Concluded.

L-58-1126

[REDACTED]

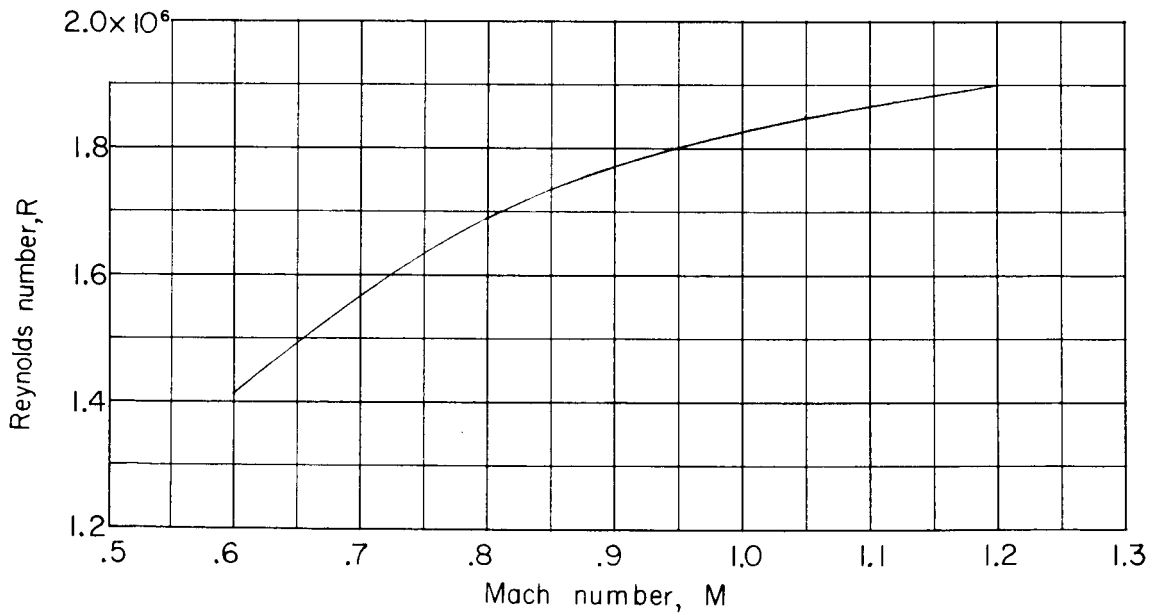
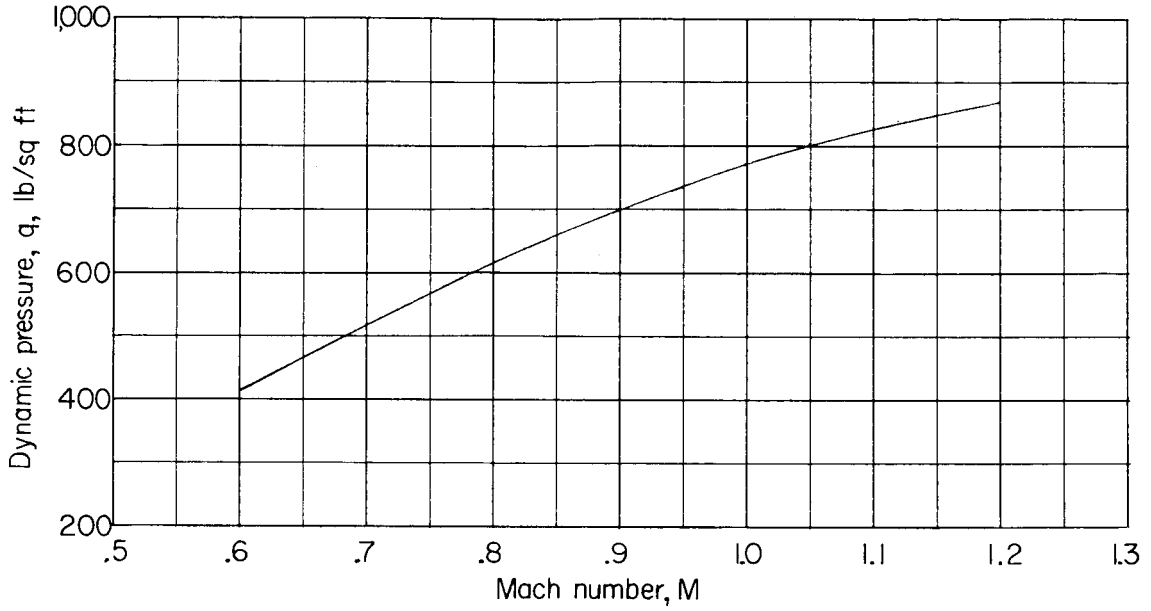
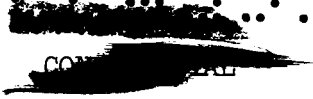
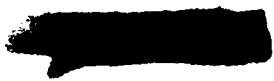
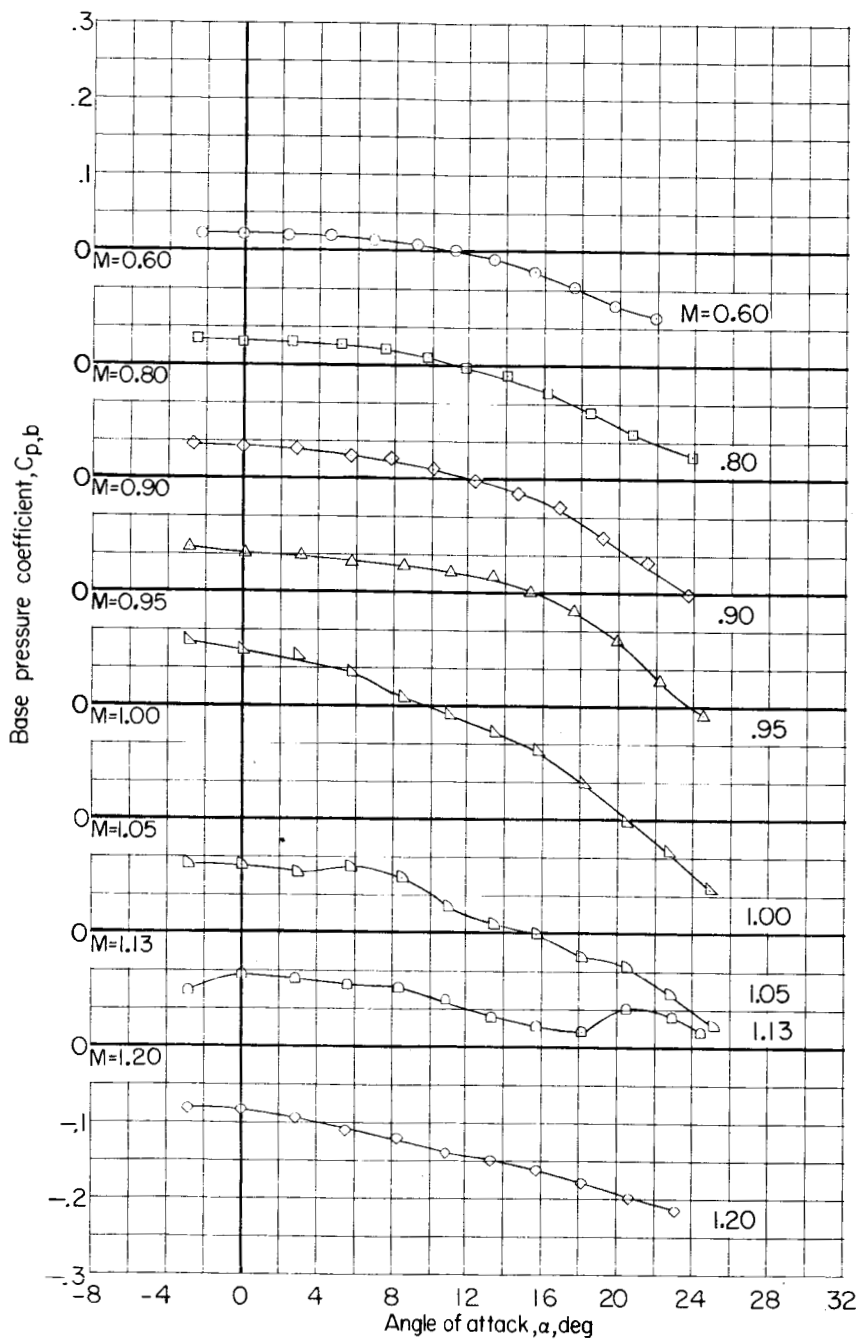


Figure 3.- Variation with Mach number of the average test dynamic pressure and Reynolds number based on the wing mean aerodynamic chord.

L-243

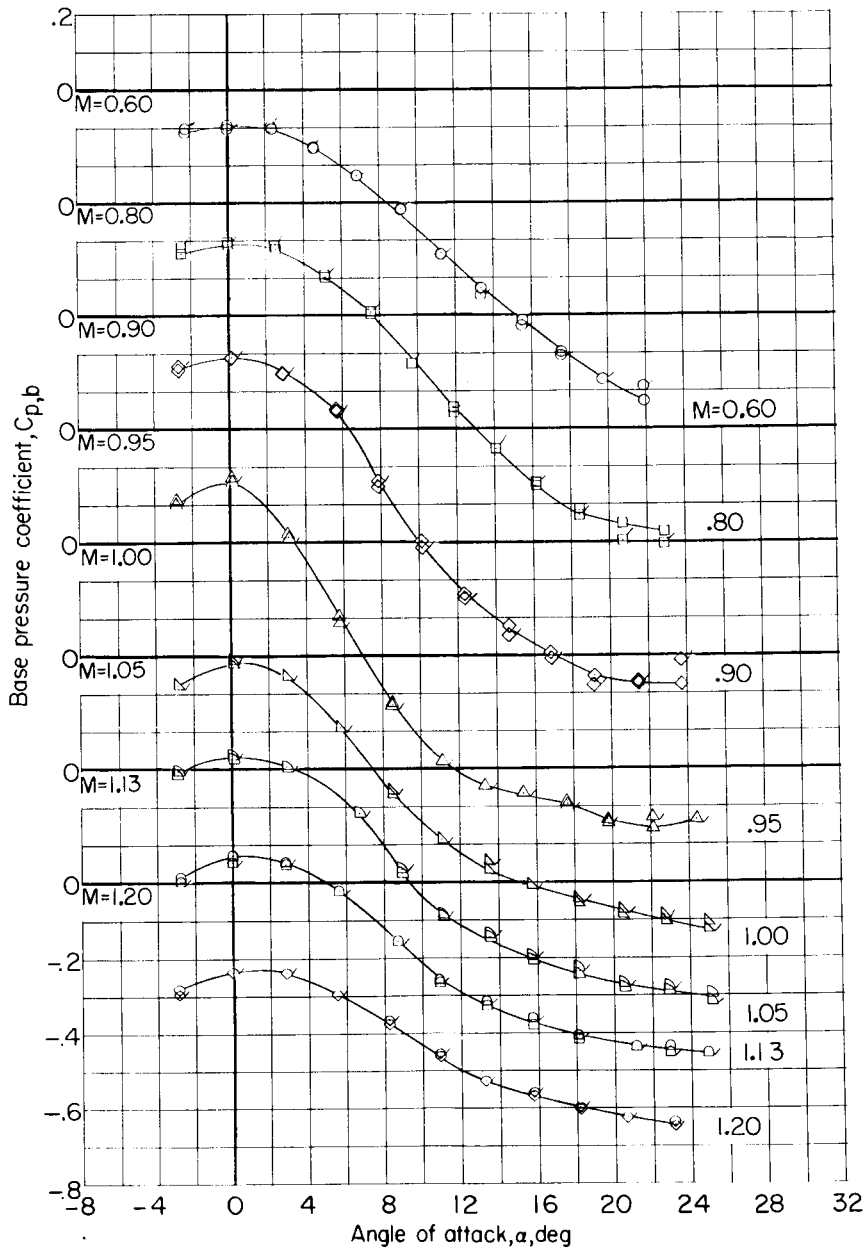


L-243



(a) Base pressure coefficients at base of fuselage.

Figure 4.- Variation of the base pressure coefficients with angle of attack.



(b) Base pressure coefficients at base of wing-tip nacelles. Plain symbols indicate values for the starboard nacelle; flagged symbols indicate values for the port nacelle.

Figure 4.- Concluded.

L-243

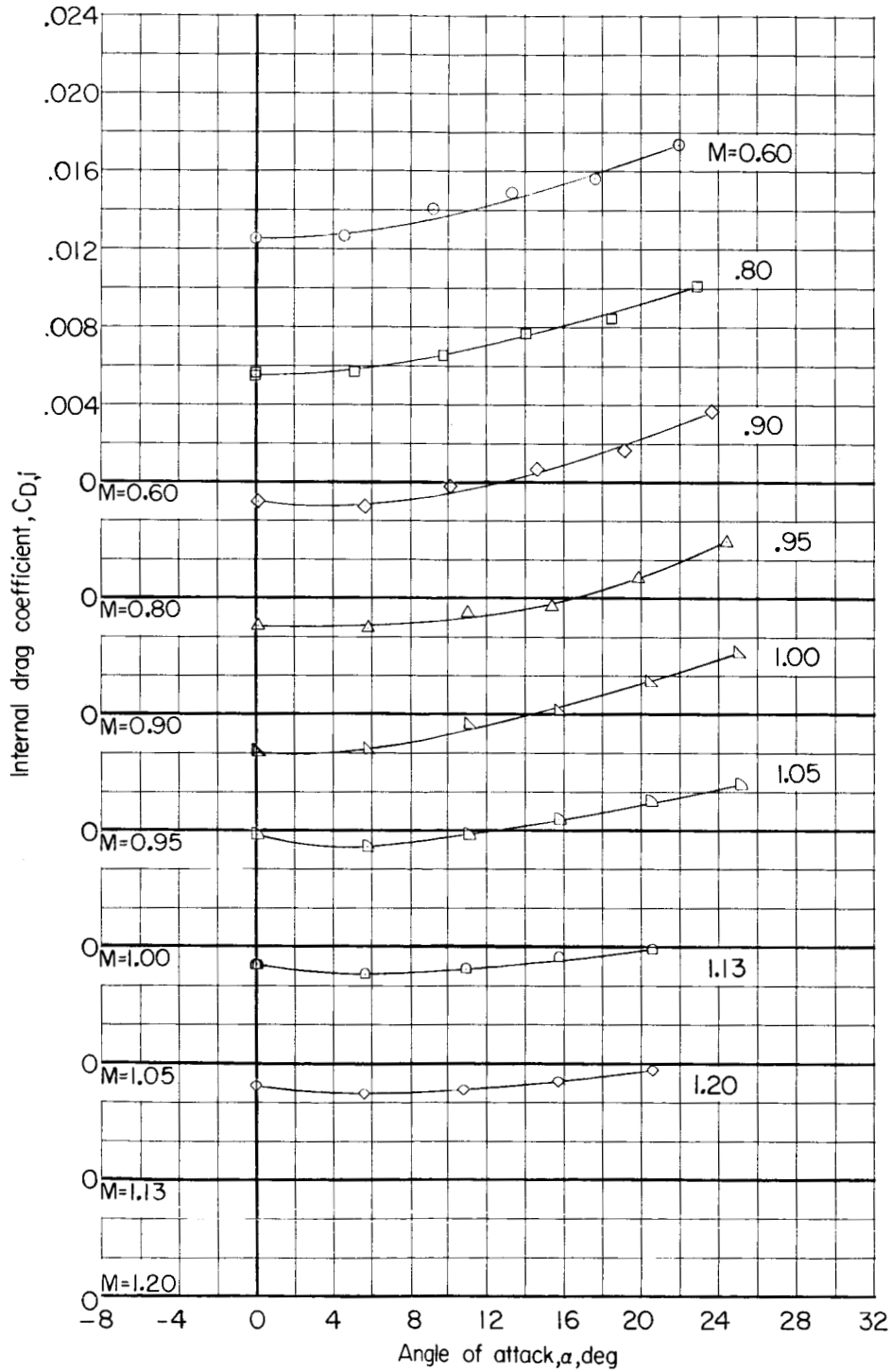


Figure 5.- Variation of the internal drag coefficient with angle of attack.



031712041030

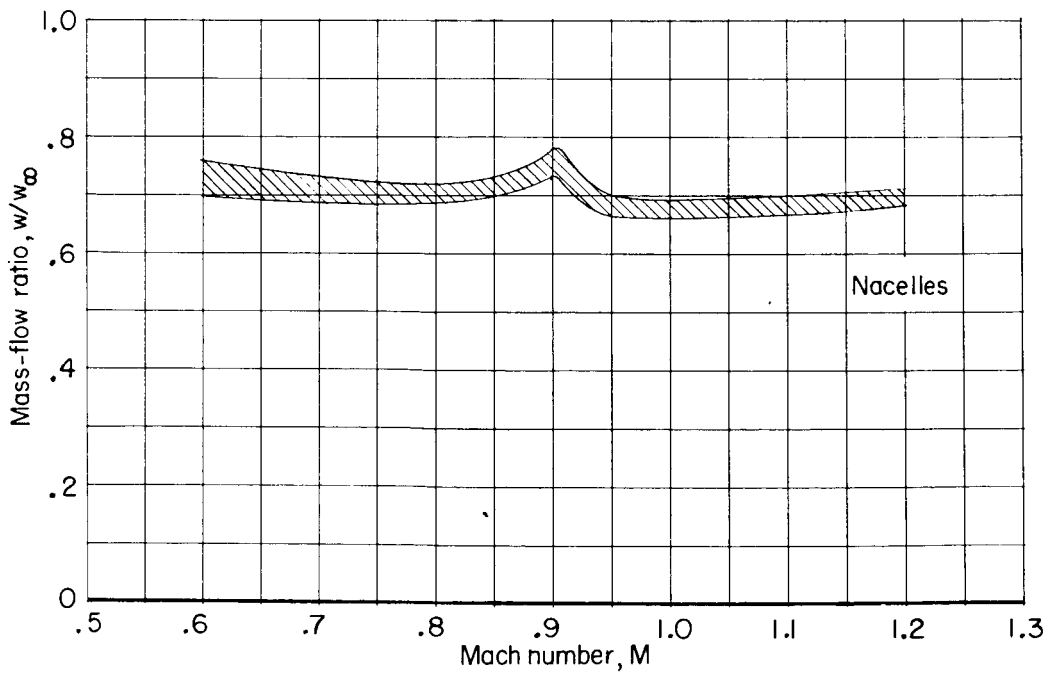
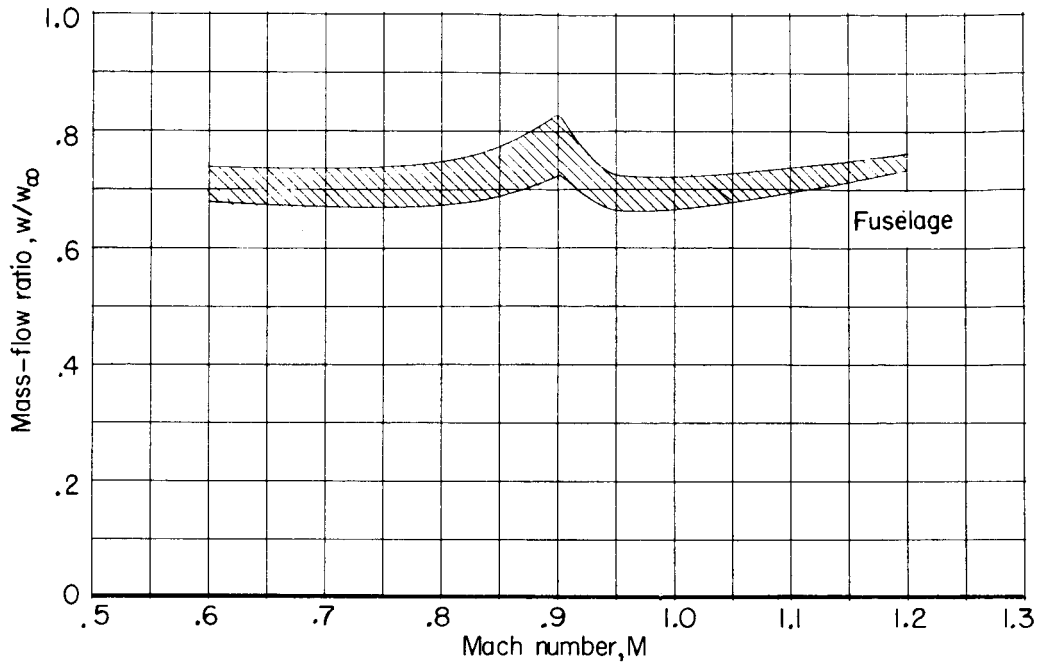


Figure 6.- Variation with Mach number of the range of mass-flow ratio for the various model configurations.

D E C L A S S I F I E D

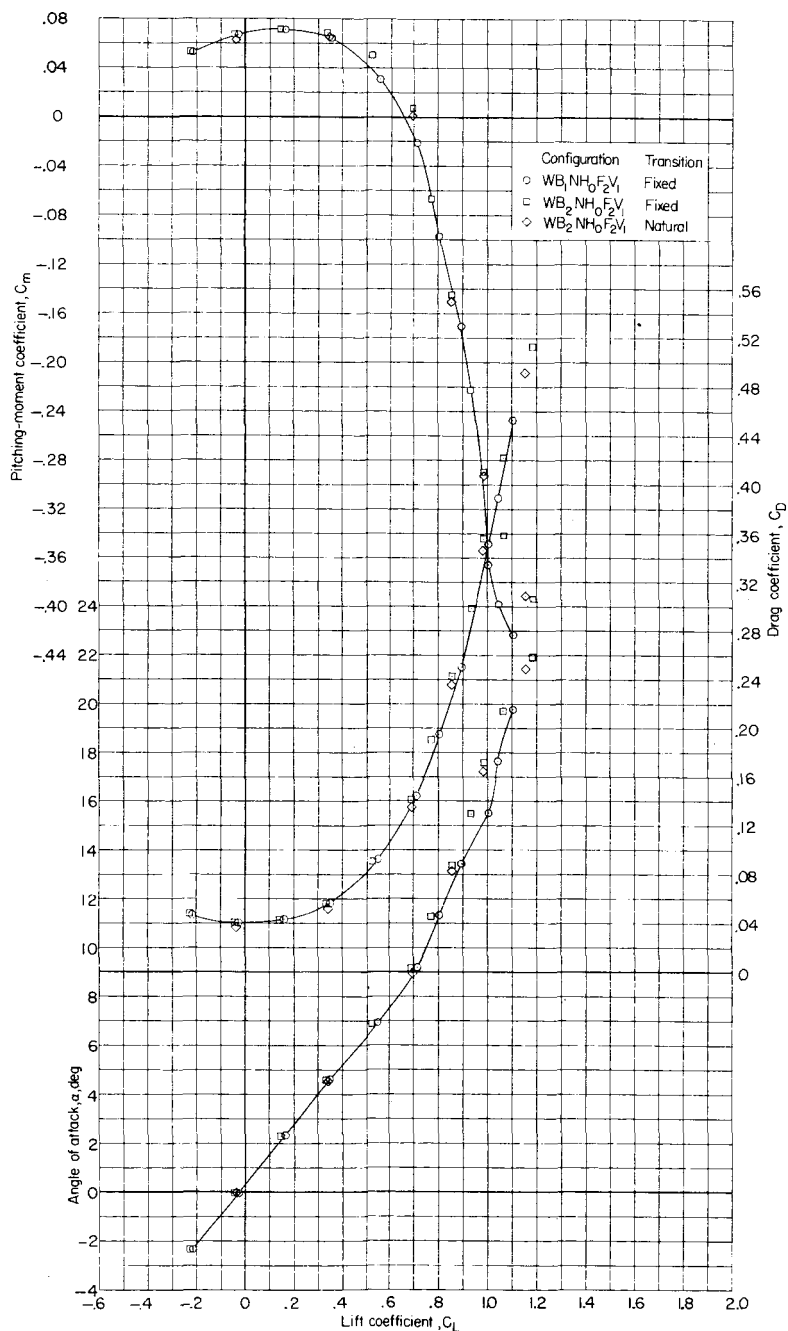
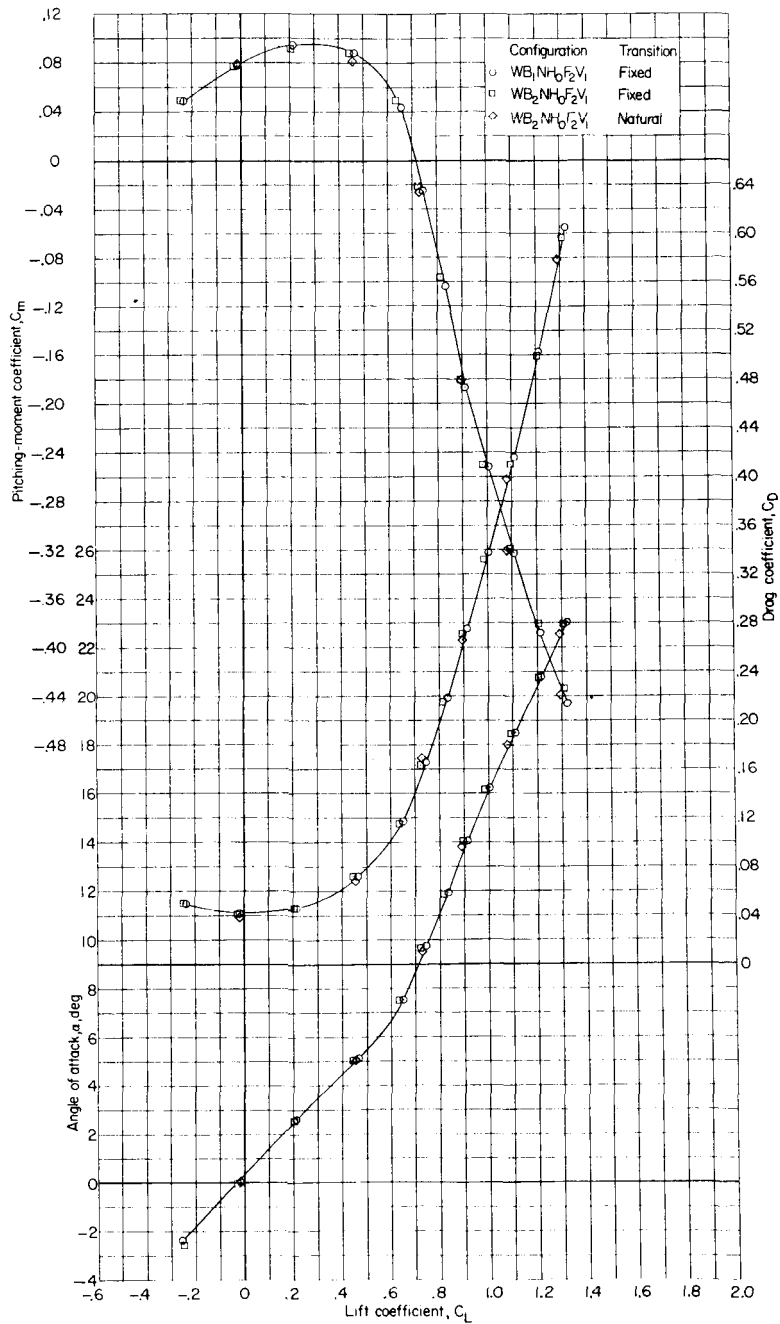
(a) $M = 0.60$.

Figure 7.- Basic aerodynamic characteristics of the model with horizontal tails having 0° dihedral.

CONFIDENTIAL

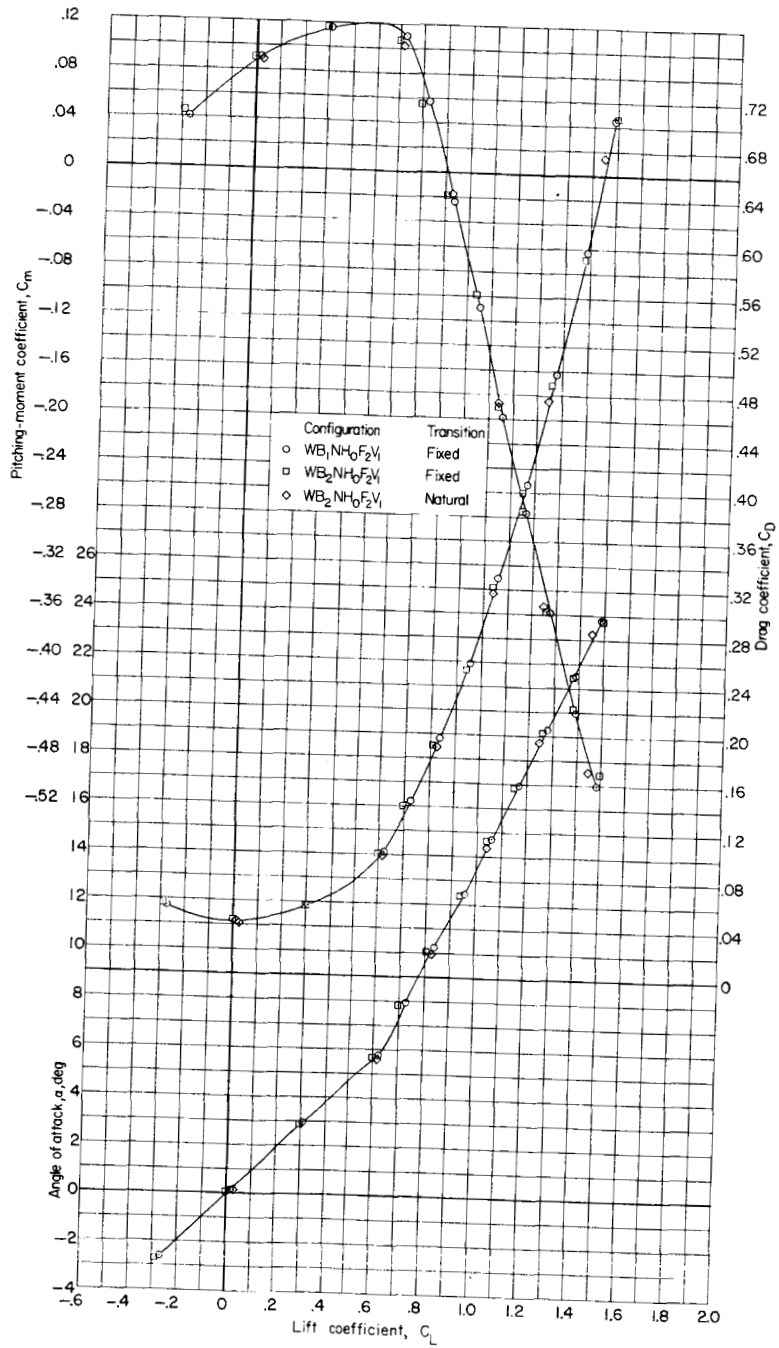


(b) $M = 0.80$.

Figure 7.- Continued.

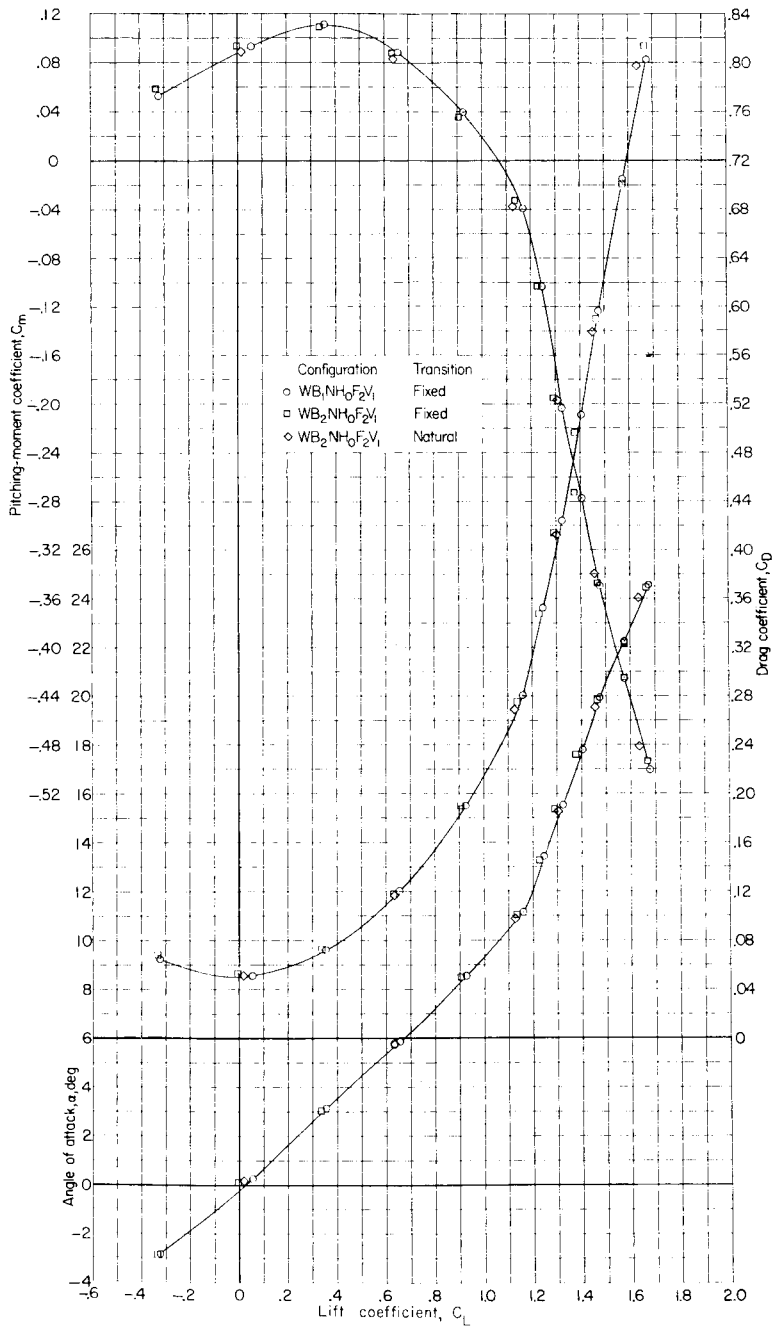
I-243

L-243



(c) $M = 0.90$.

Figure 7.- Continued.

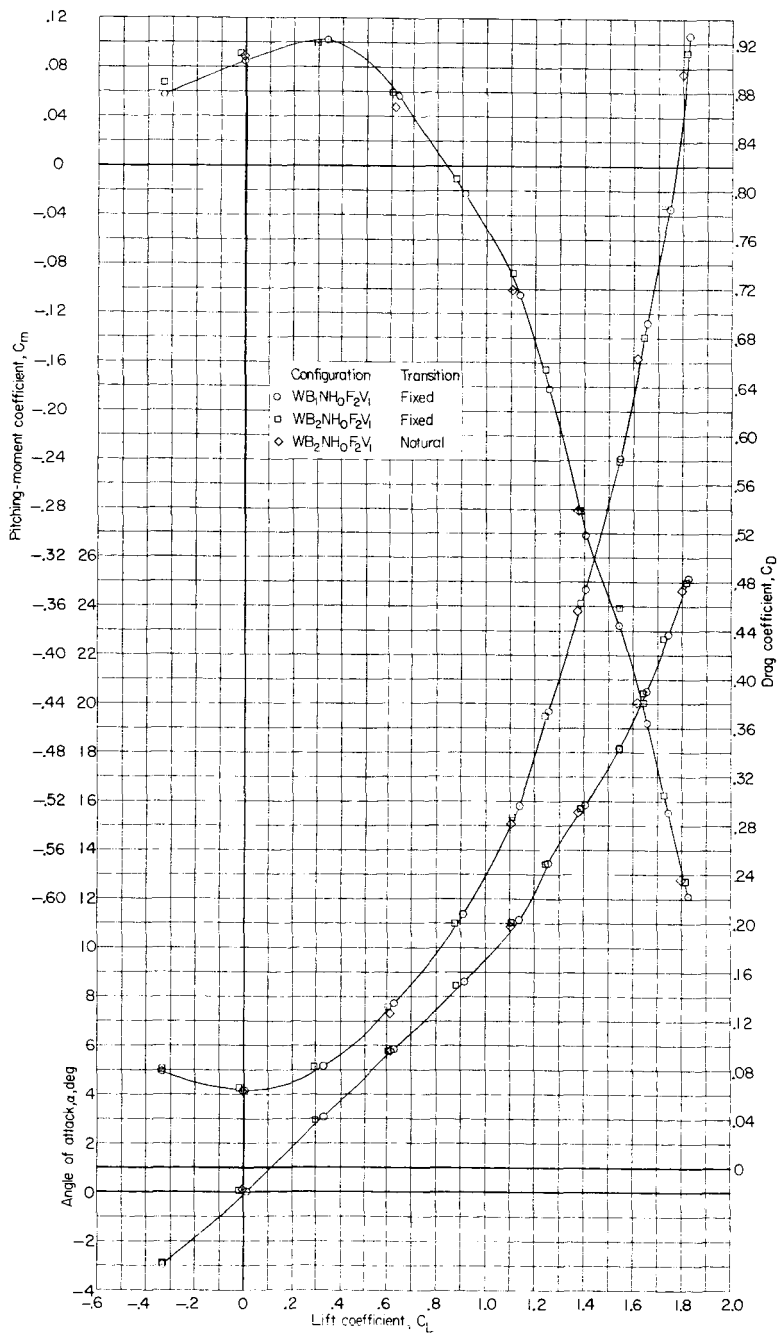


(d) $M = 0.95$.

Figure 7.- Continued.

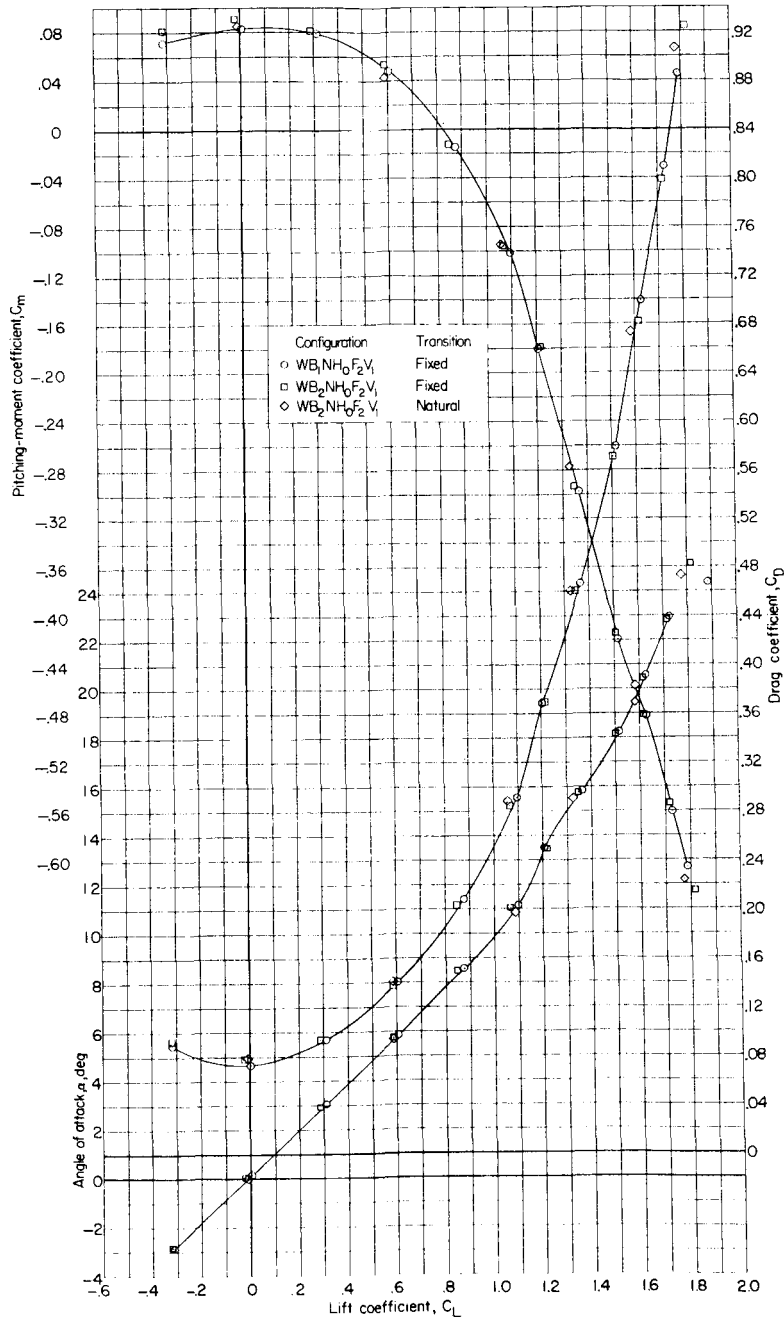
I-243

L-243



(e) $M = 1.00$.

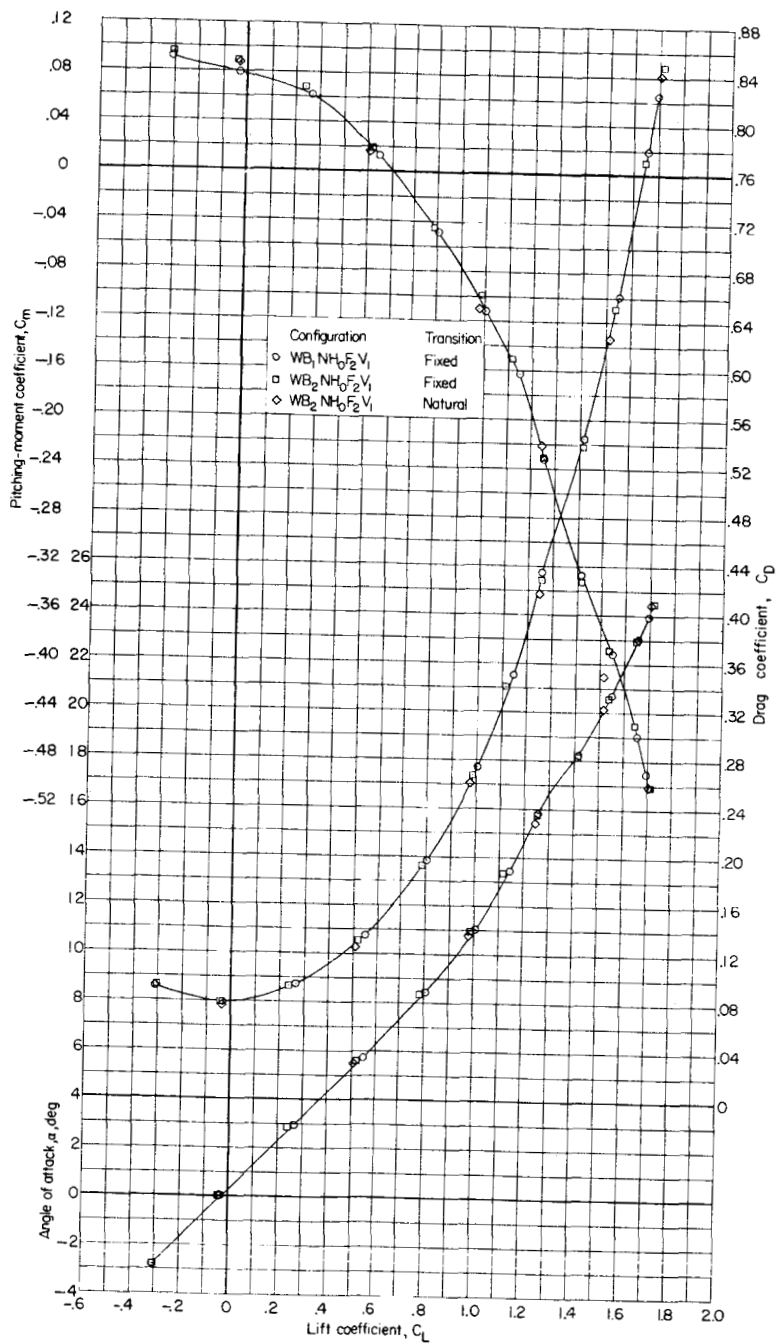
Figure 7.- Continued.



(f) $M = 1.05$.

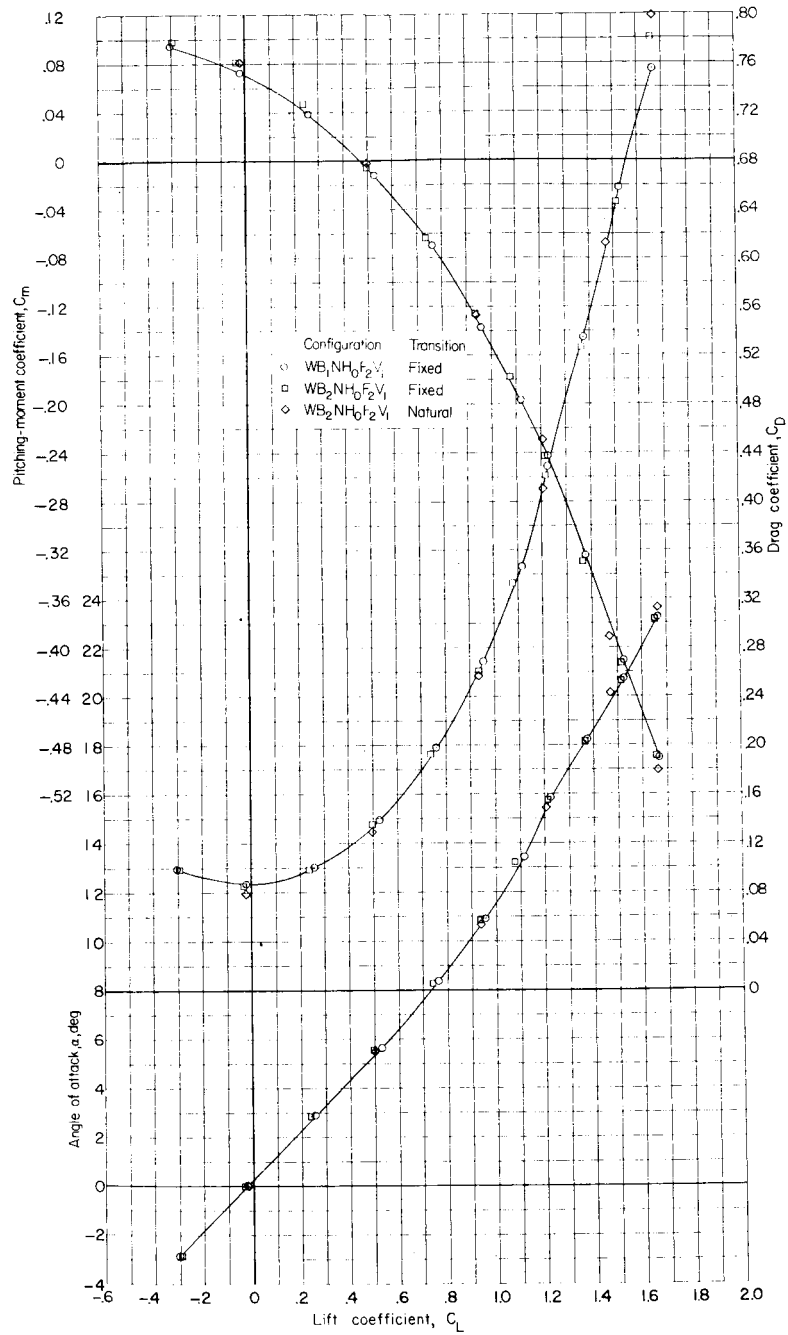
Figure 7.- Continued.

I-243



(g) $M = 1.13$.

Figure 7.- Continued.



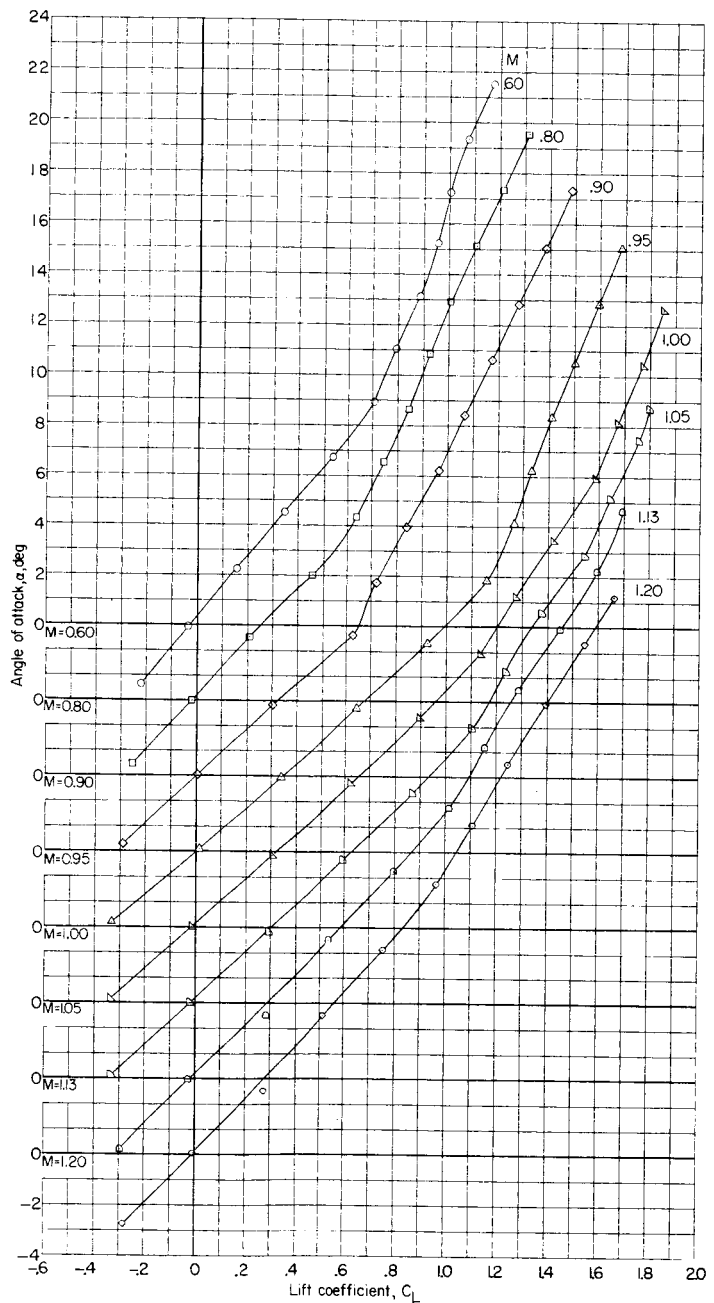
(h) $M = 1.20$.

Figure 7.- Concluded.

L-243

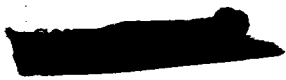


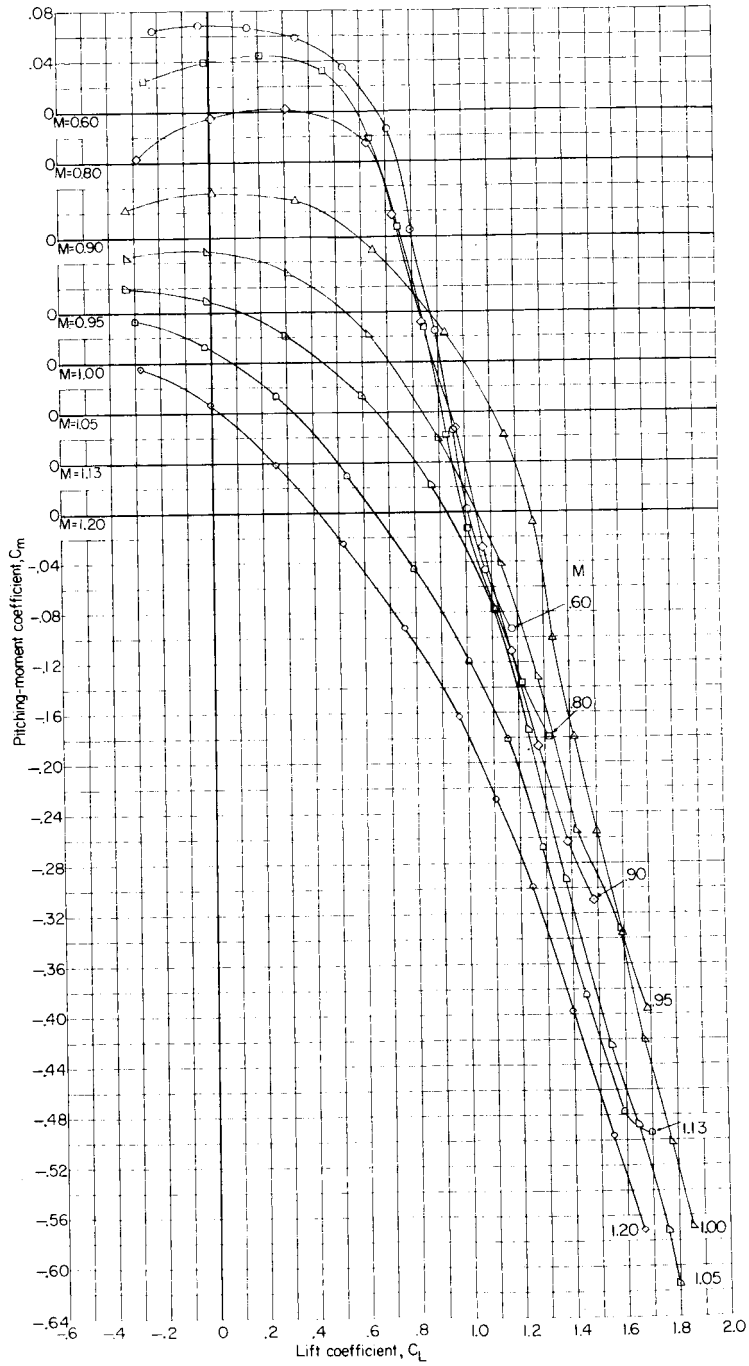
L-243



(a) Effect of α on C_L .

Figure 8.- Basic aerodynamic characteristics of the model with horizontal tails having -15° dihedral.



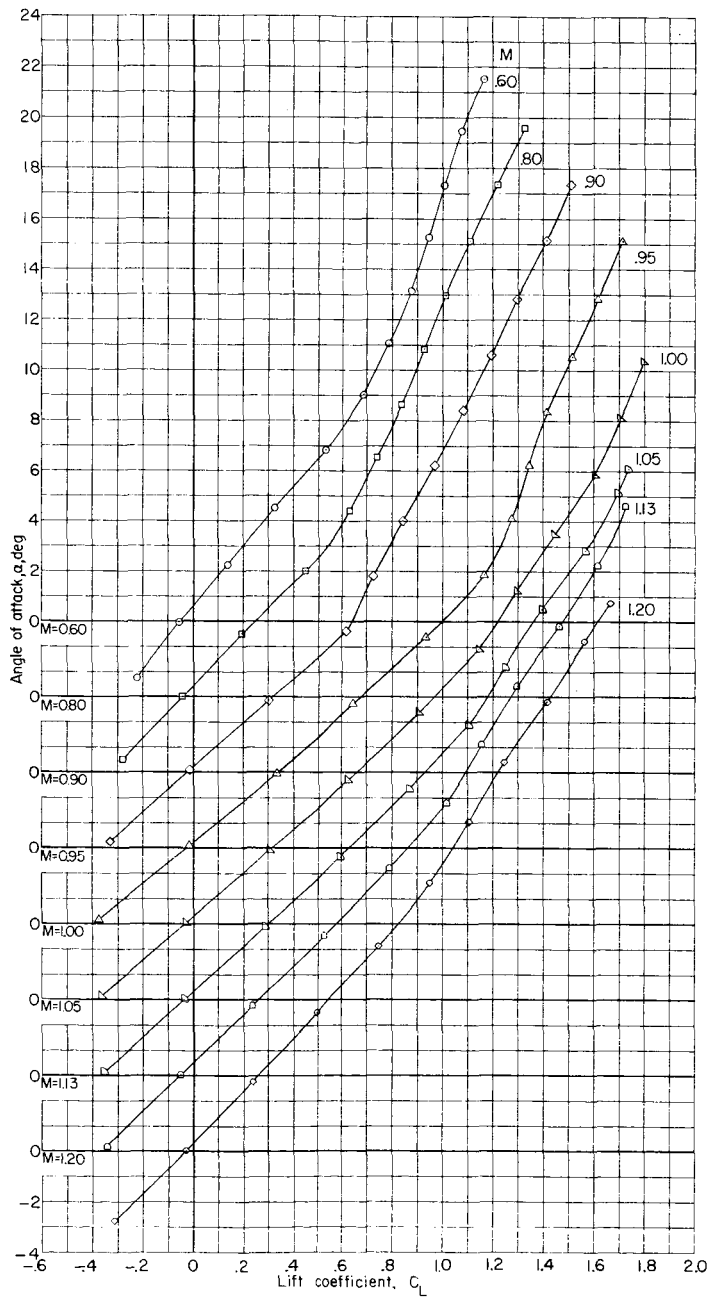


L-243

(b) Variation of C_m with C_L .

Figure 8.- Continued.





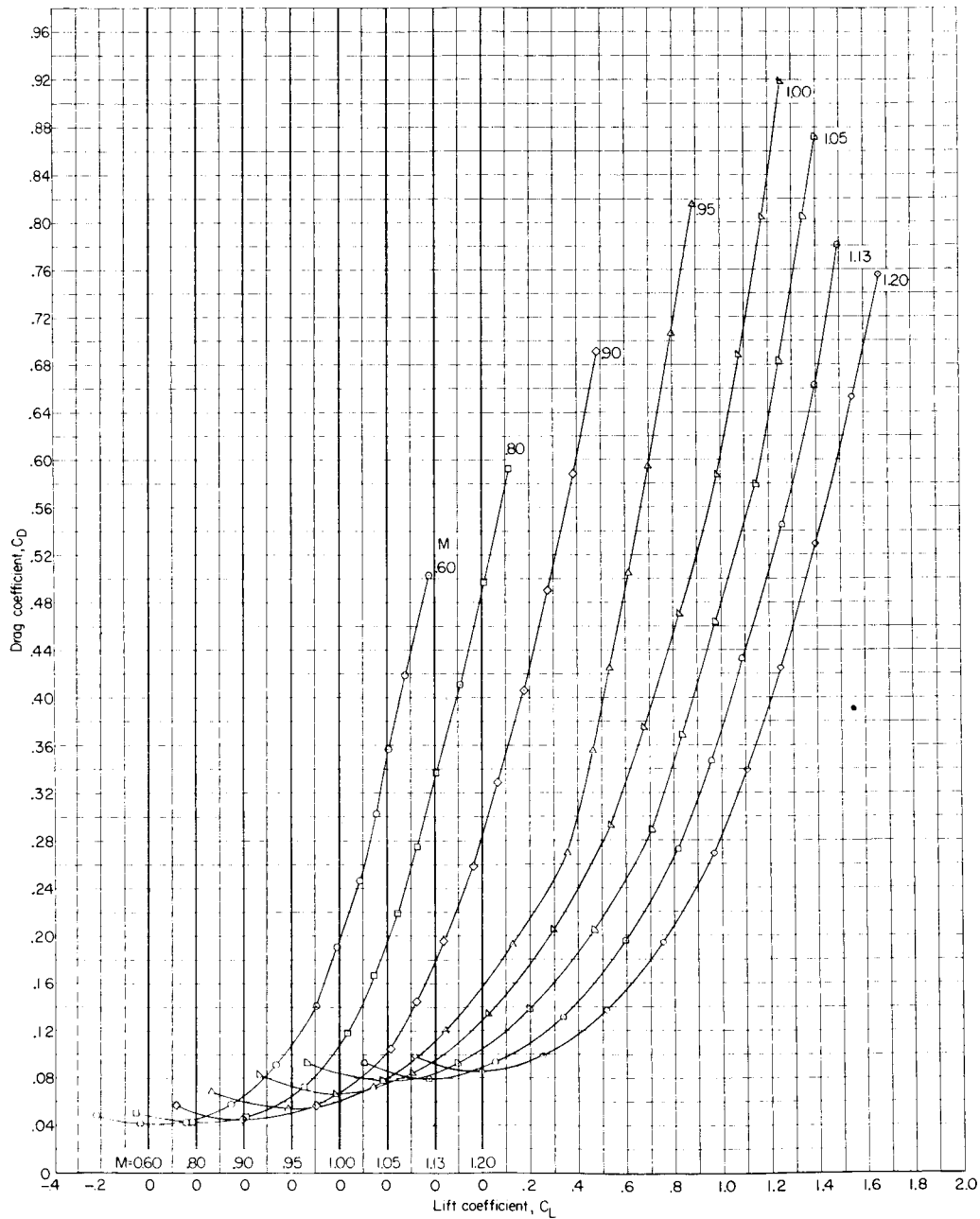
L-213

(a) Effect of α on C_L .

Figure 9.- Basic aerodynamic characteristics of the model with horizontal tails having -30° dihedral.



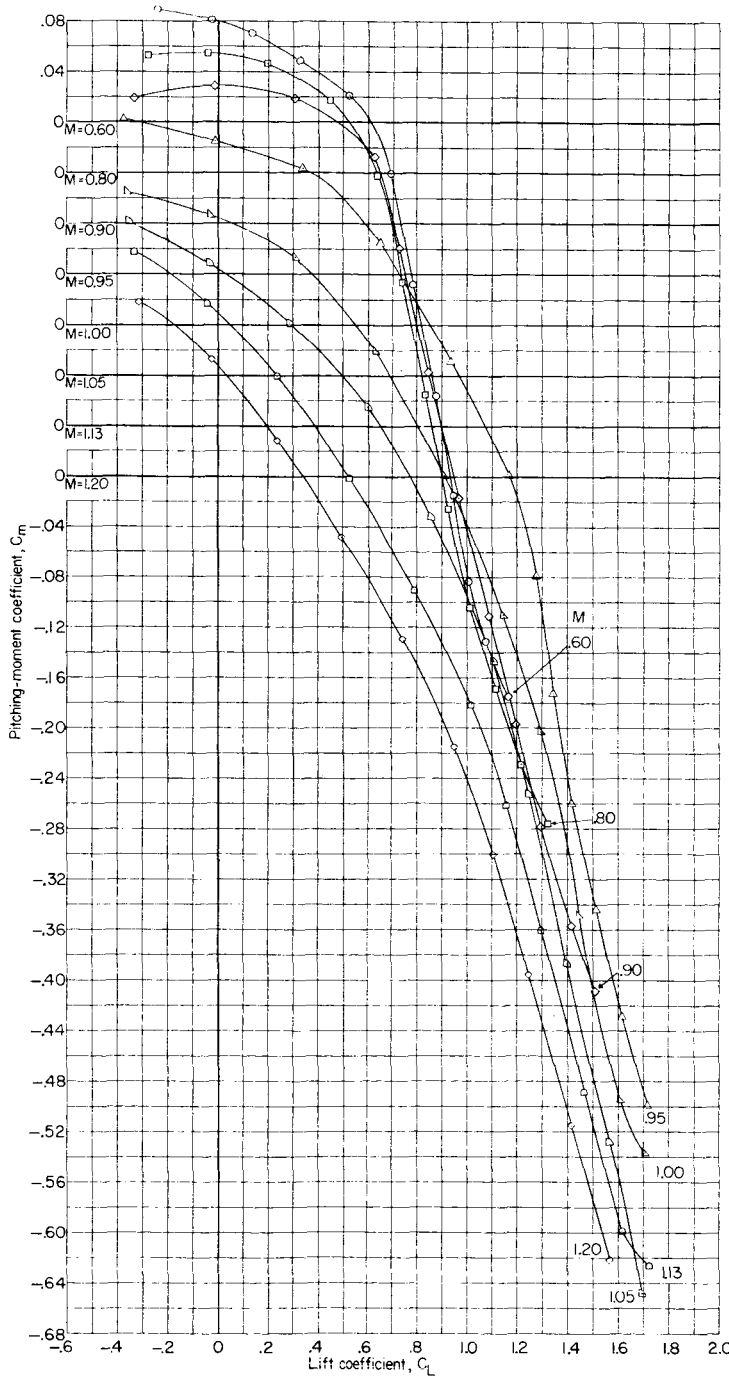
L-243



(c) Variation of C_D with C_L .

Figure 8.- Concluded.

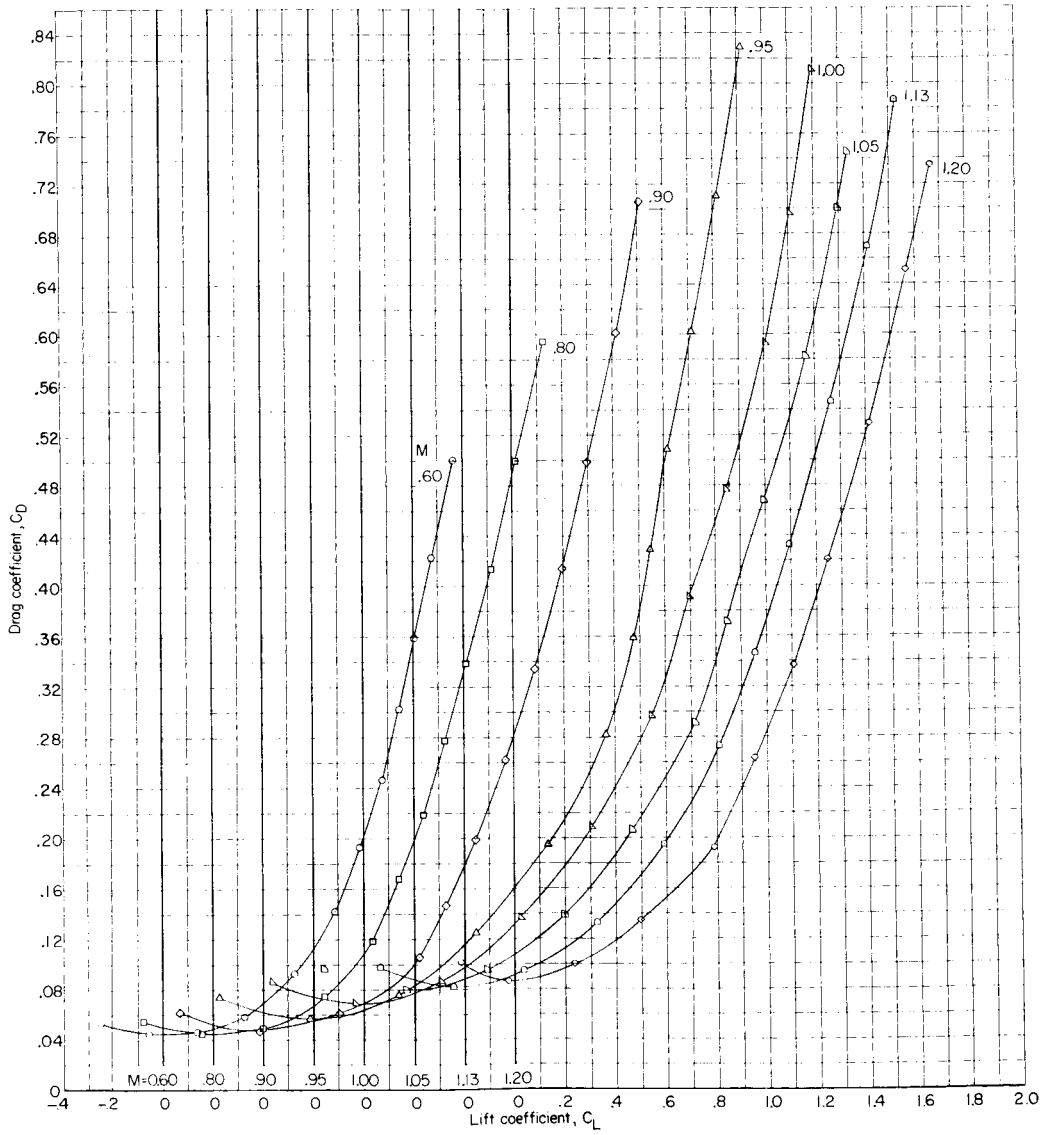




L-243

(b) Variation of C_m with C_L .

Figure 9.- Continued.

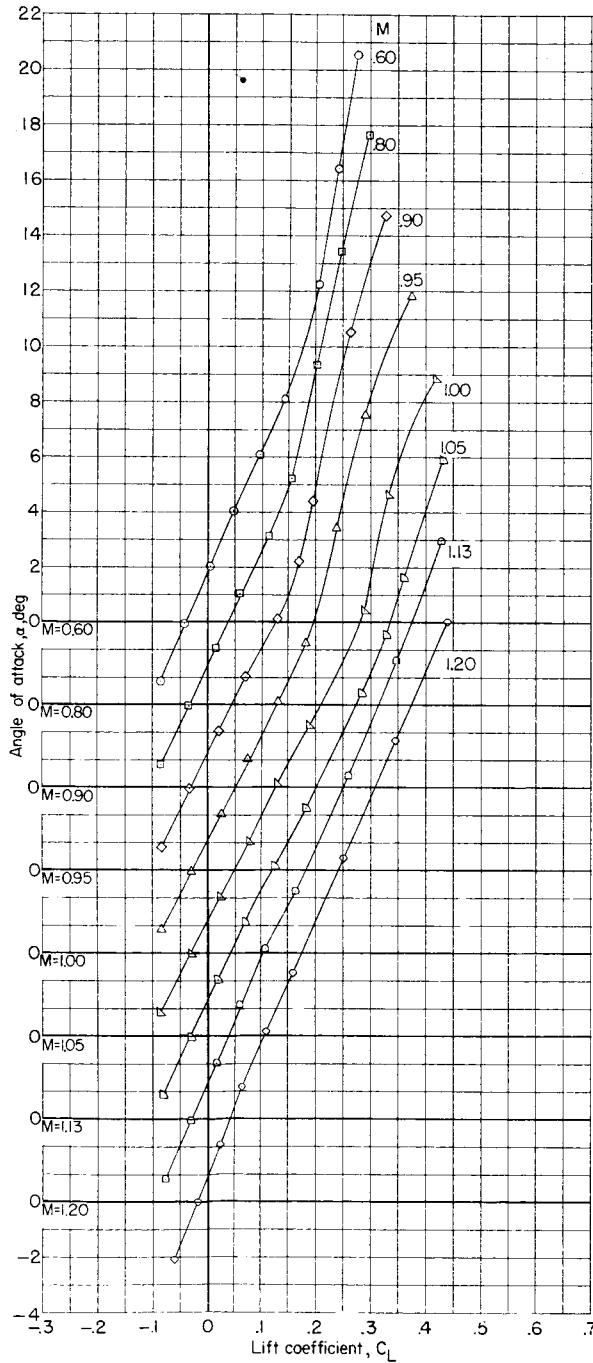
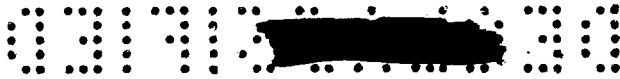


(c) Variation of C_D with C_L .

Figure 9.- Concluded.

I-243

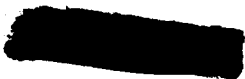




L-243

(a) Configuration B₂H₀F₂V₁.

Figure 11.- Variation with lift coefficient of angle of attack for the model with wing off.



L-243

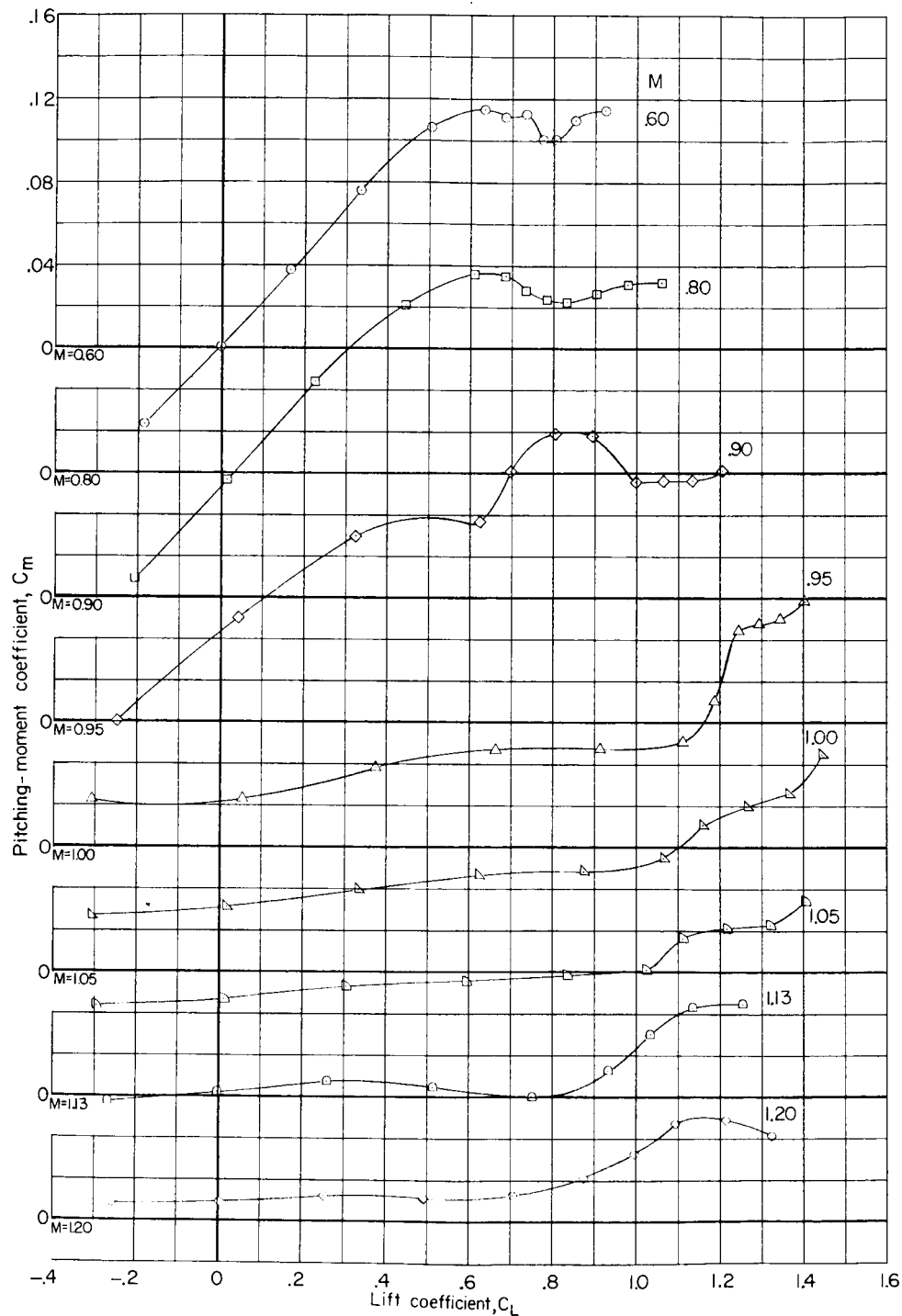
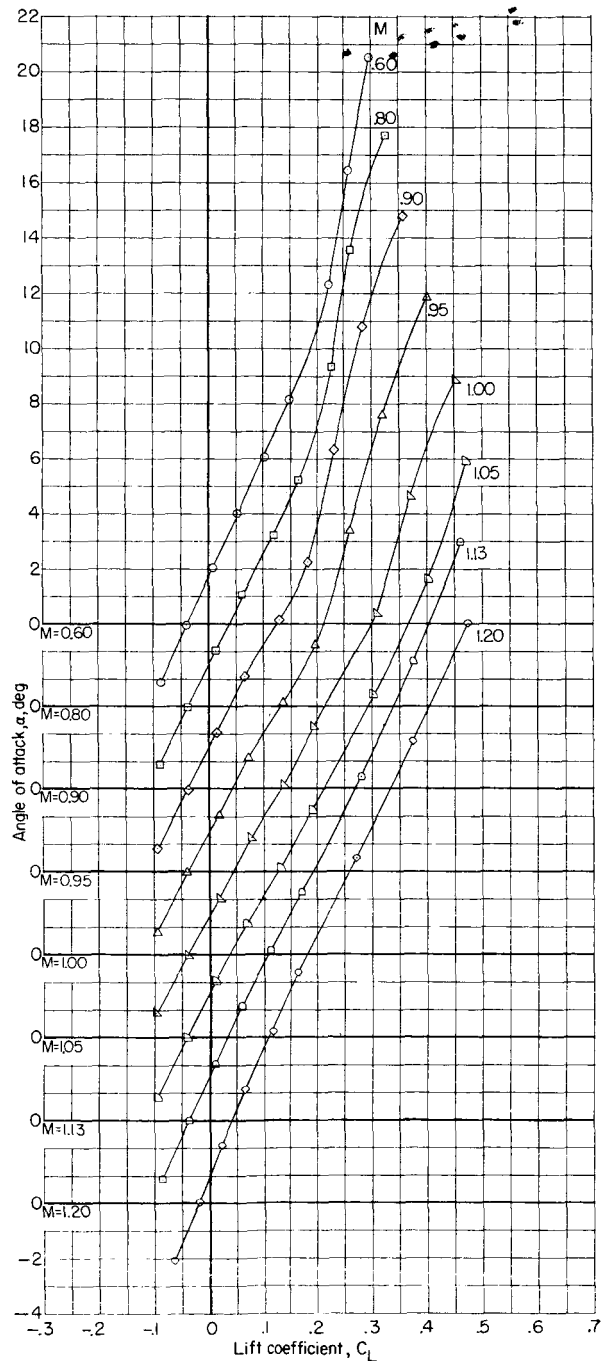


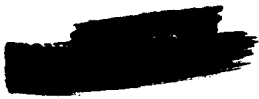
Figure 10.- Variation with lift coefficient of pitching-moment coefficient for the model with horizontal tails off.

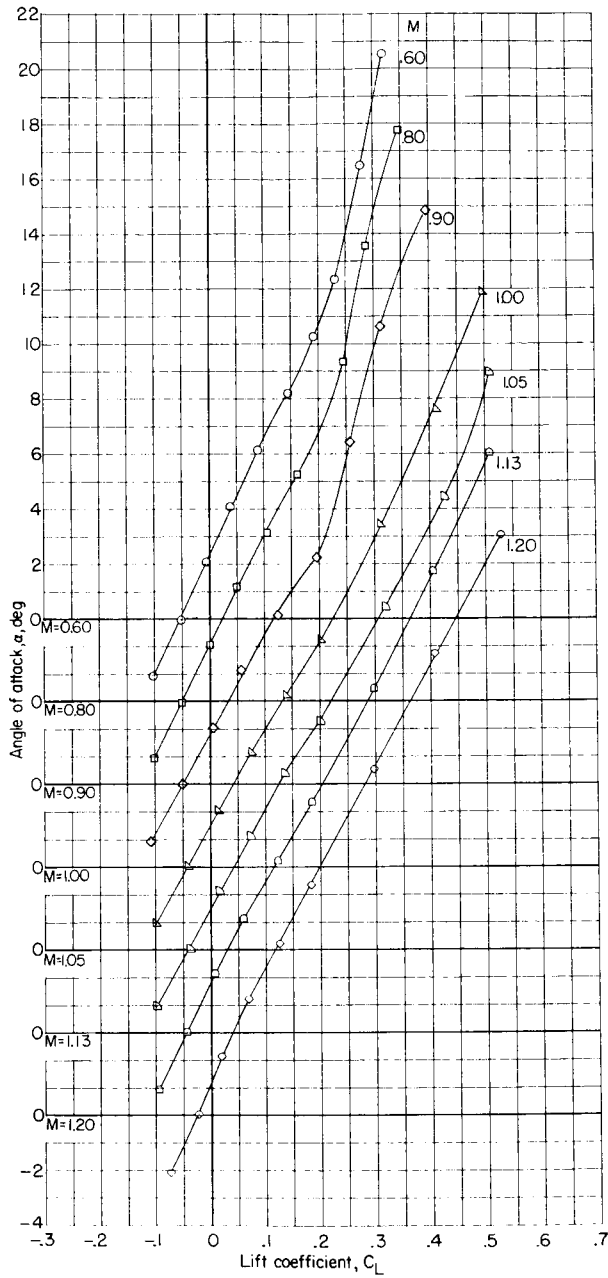
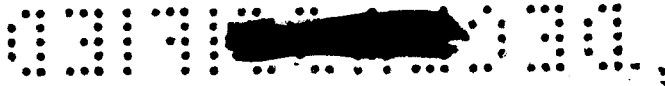
L-243



(b) Configuration B₂H₁₅F₁V₁.

Figure 11.- Continued.





L-243

(c) Configuration B₂H₃₀V₁.

Figure 11.- Concluded.



SECRET

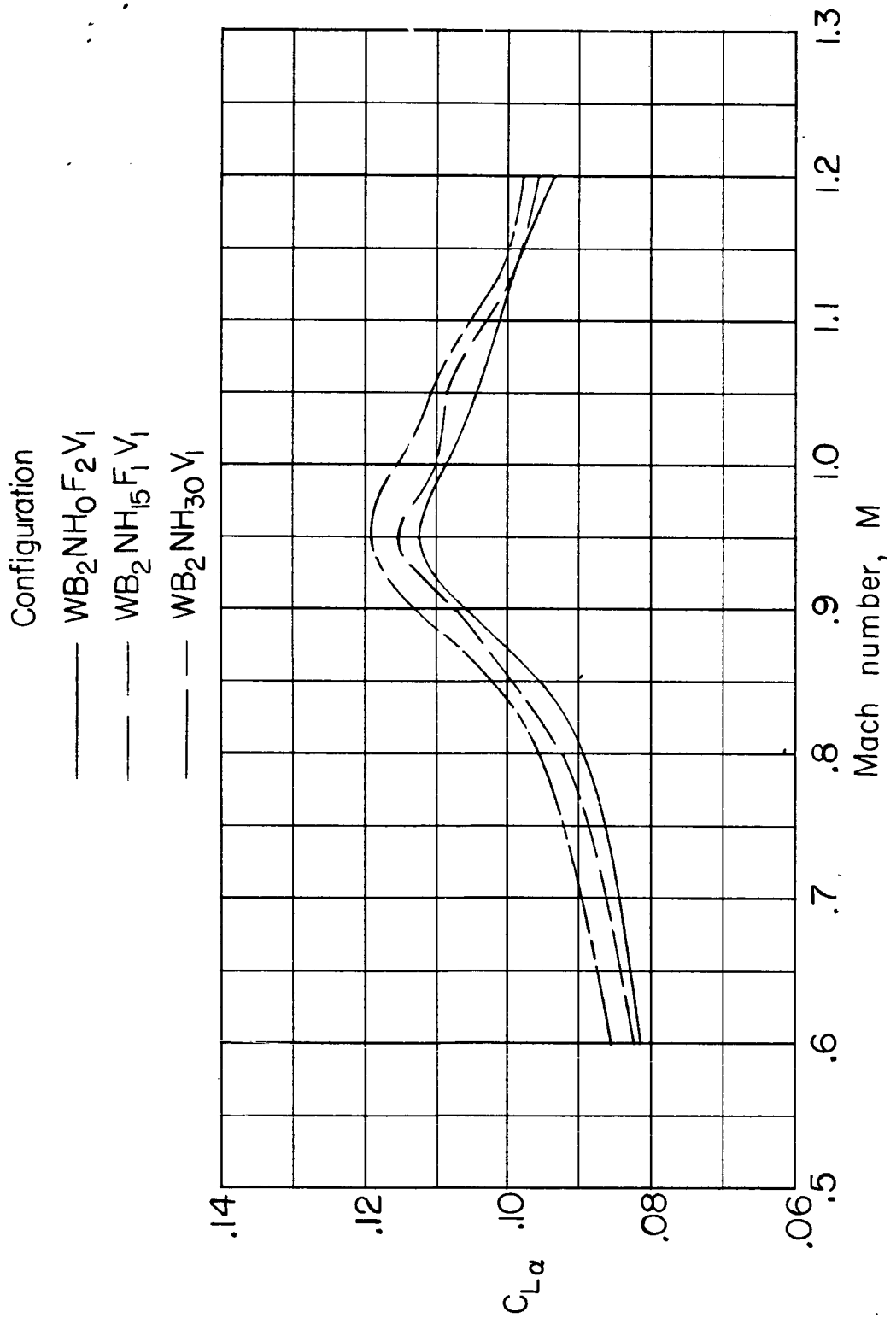
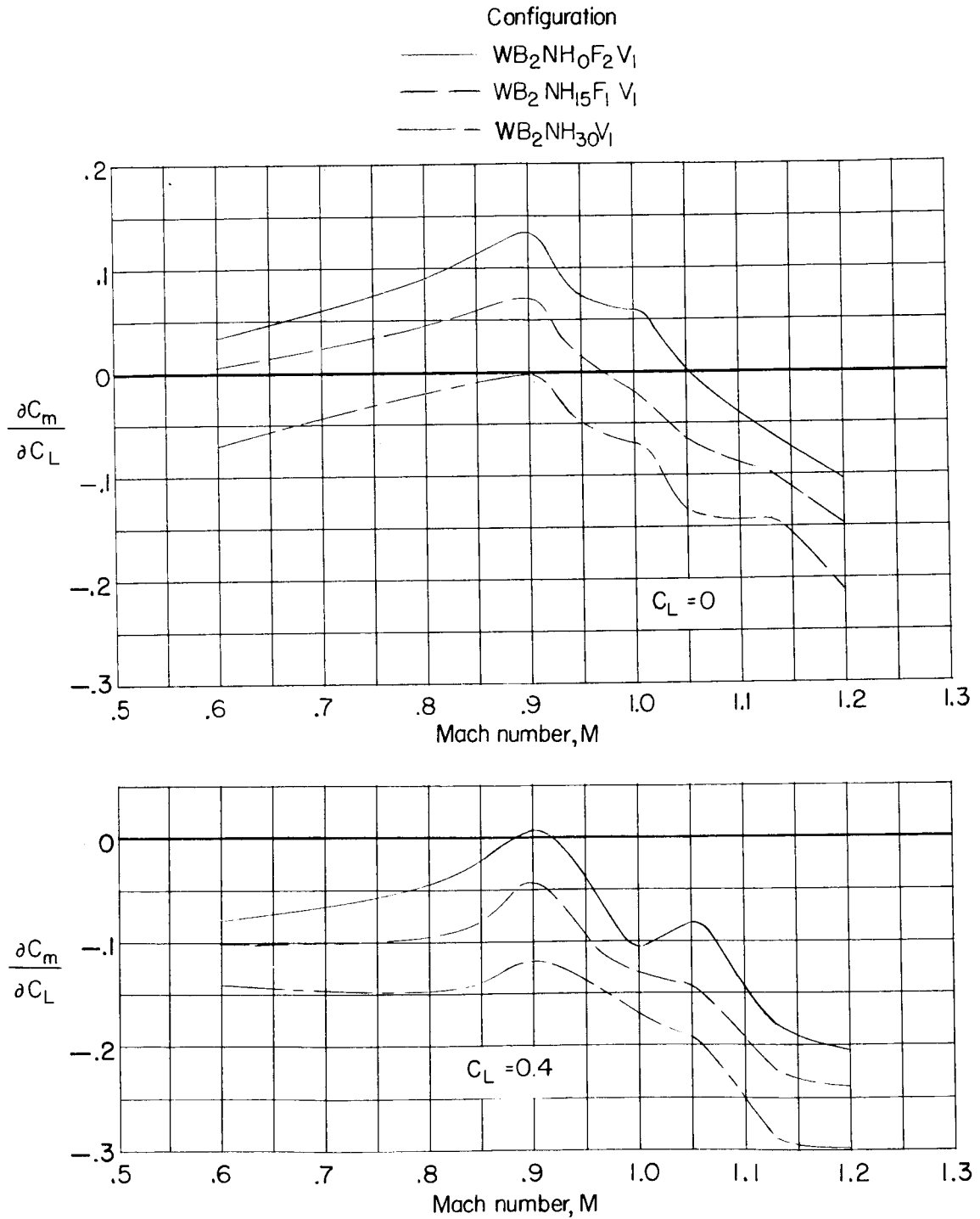
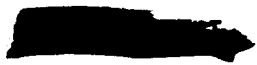


Figure 12.- Variation with Mach number of lift-curve slope.



I-243

Figure 13.- Variation with Mach number of the static-longitudinal-stability parameter.



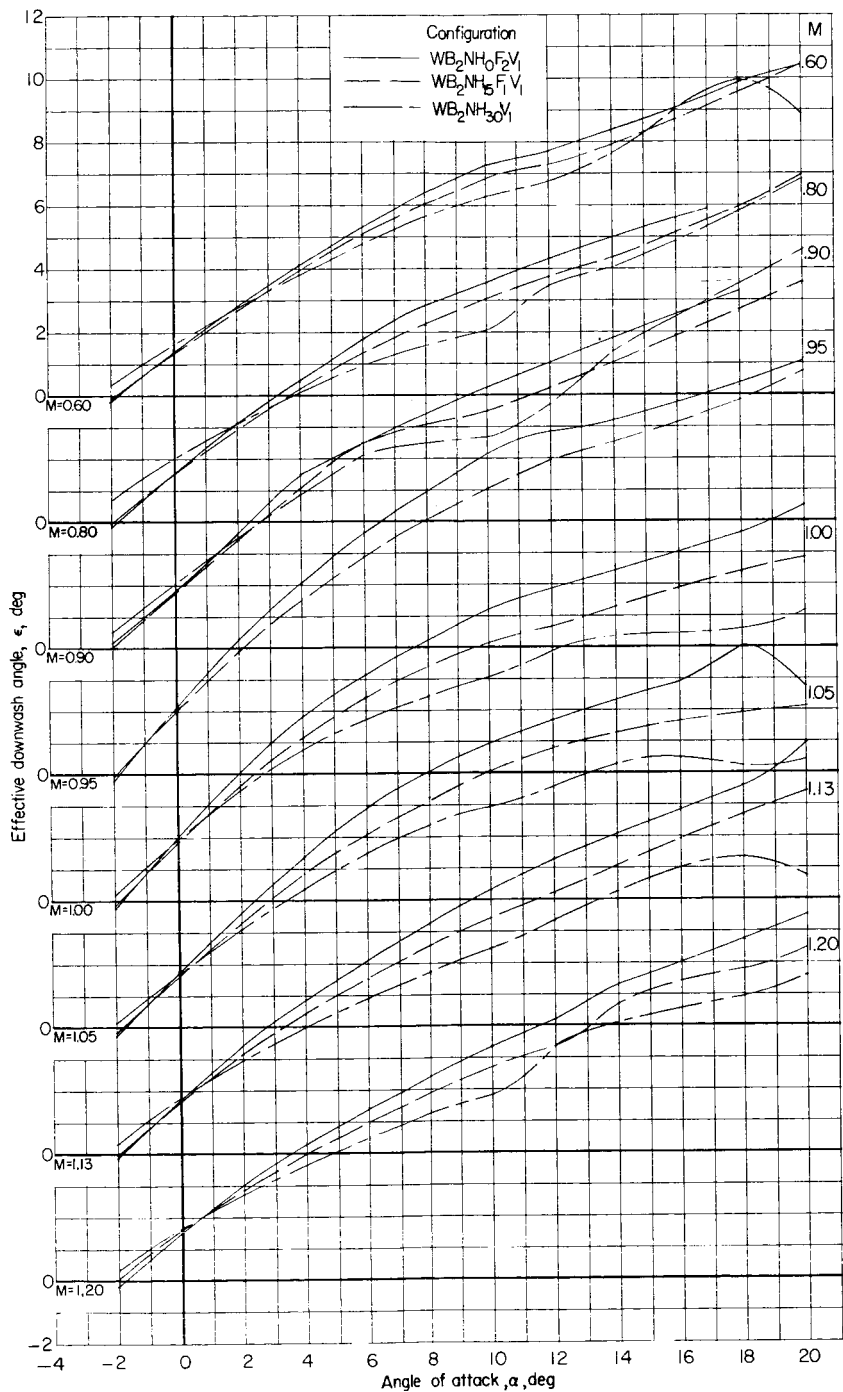


Figure 14.- Variation with angle of attack of effective downwash angle at the horizontal tail.

L-243

SECRET

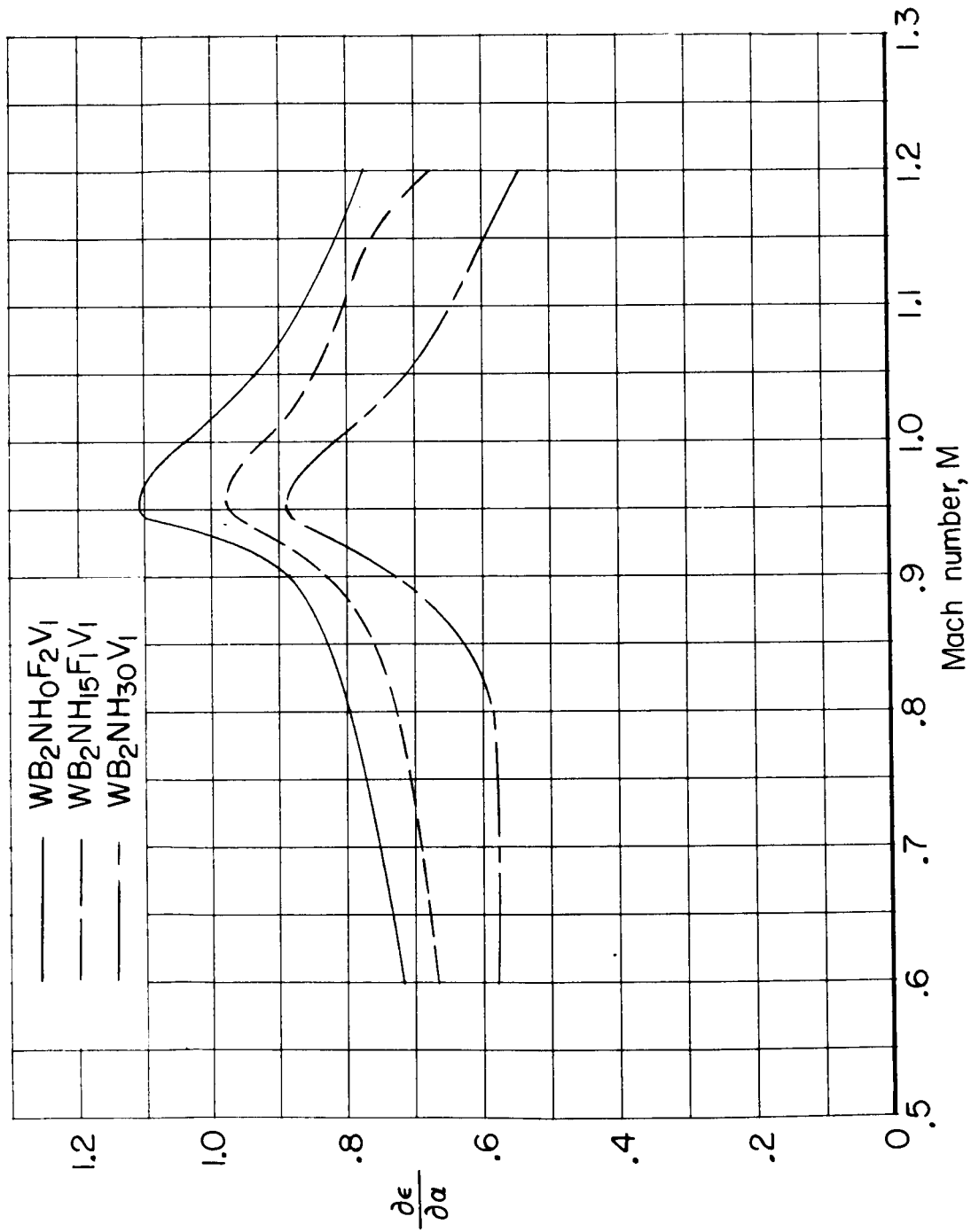


Figure 15.- Variation with Mach number of the average rate of change of downwash angle with angle of attack at the horizontal tail. $\alpha = -2^\circ$ to 4° .

I-243

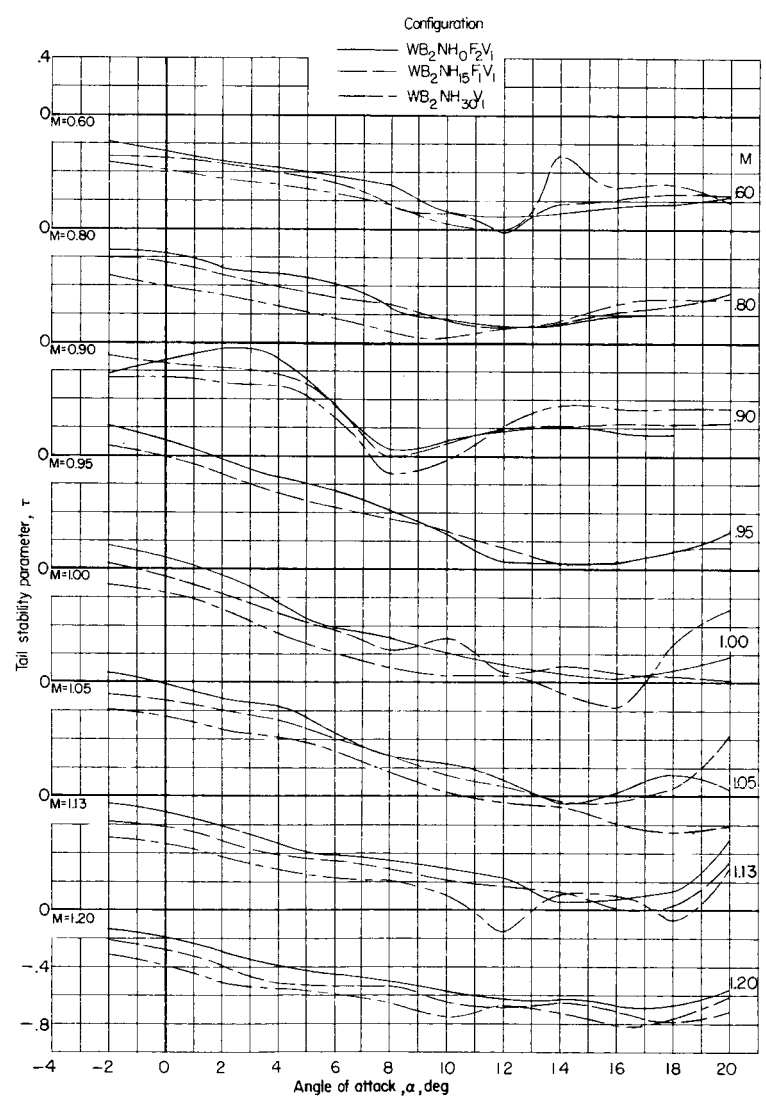


Figure 16.- Variation with angle of attack of tail stability parameter.



CONFIDENTIAL

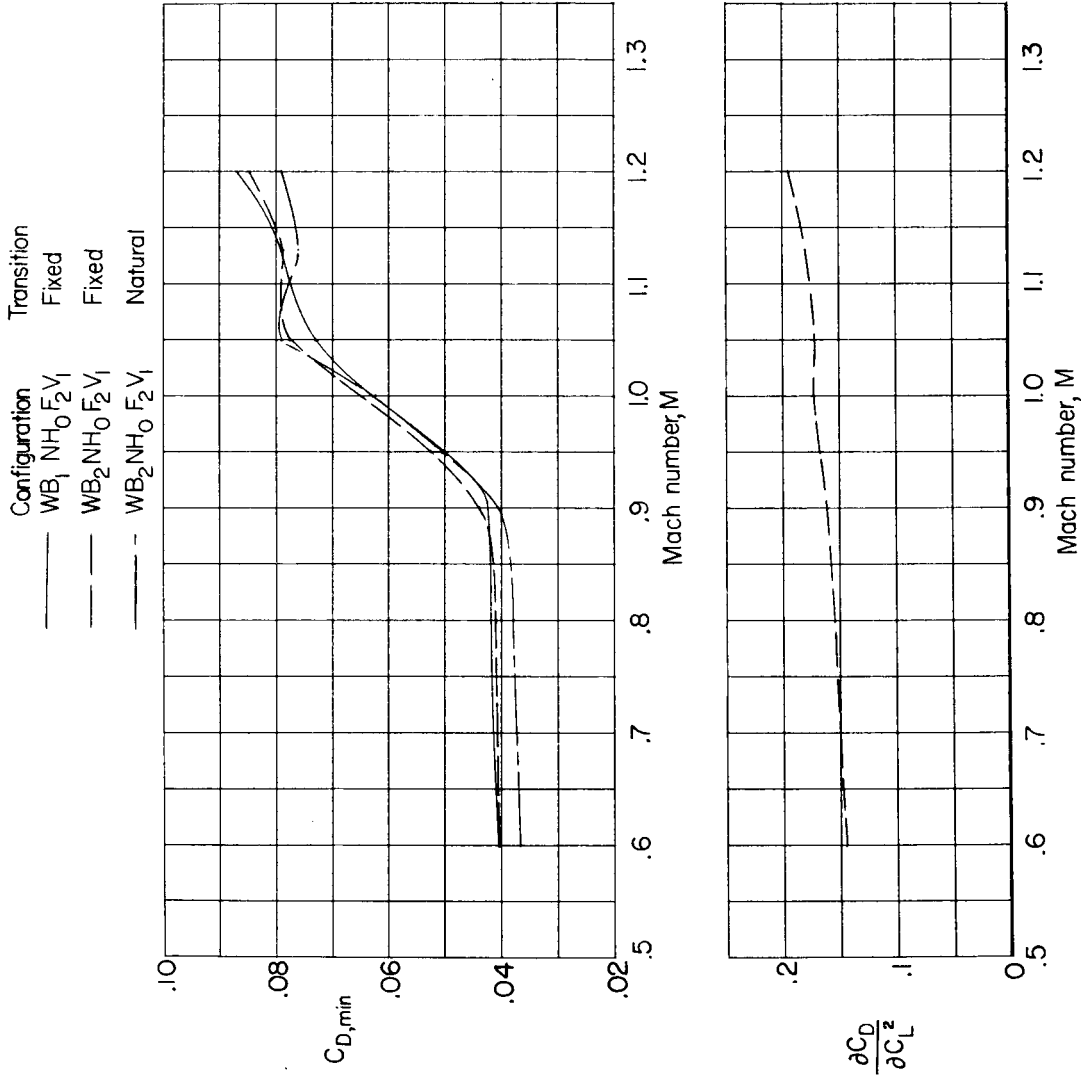


Figure 17.- Variation with Mach number of minimum drag coefficient and drag-due-to-lift factor.

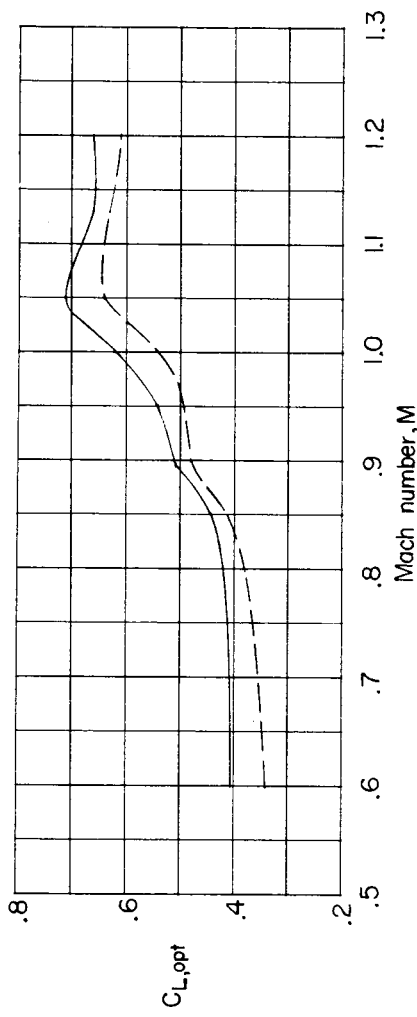
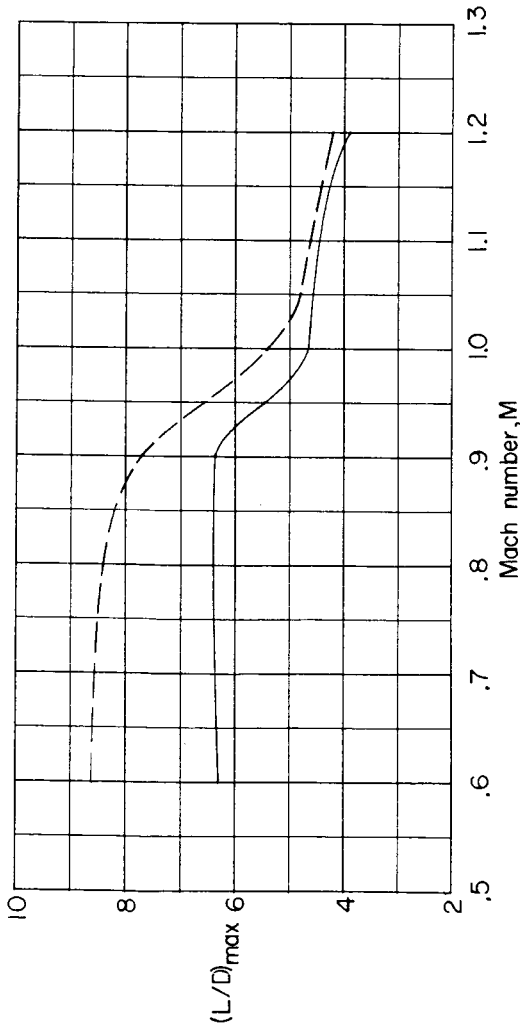


Figure 18.- Variation with Mach number of maximum lift-drag ratio and lift coefficient for maximum lift-drag ratio. Configuration $WB_{2}NH_{0}F_{2}V_{1}$; dashed lines indicate values adjusted to a Reynolds number of 20×10^6 .

CONFIDENTIAL

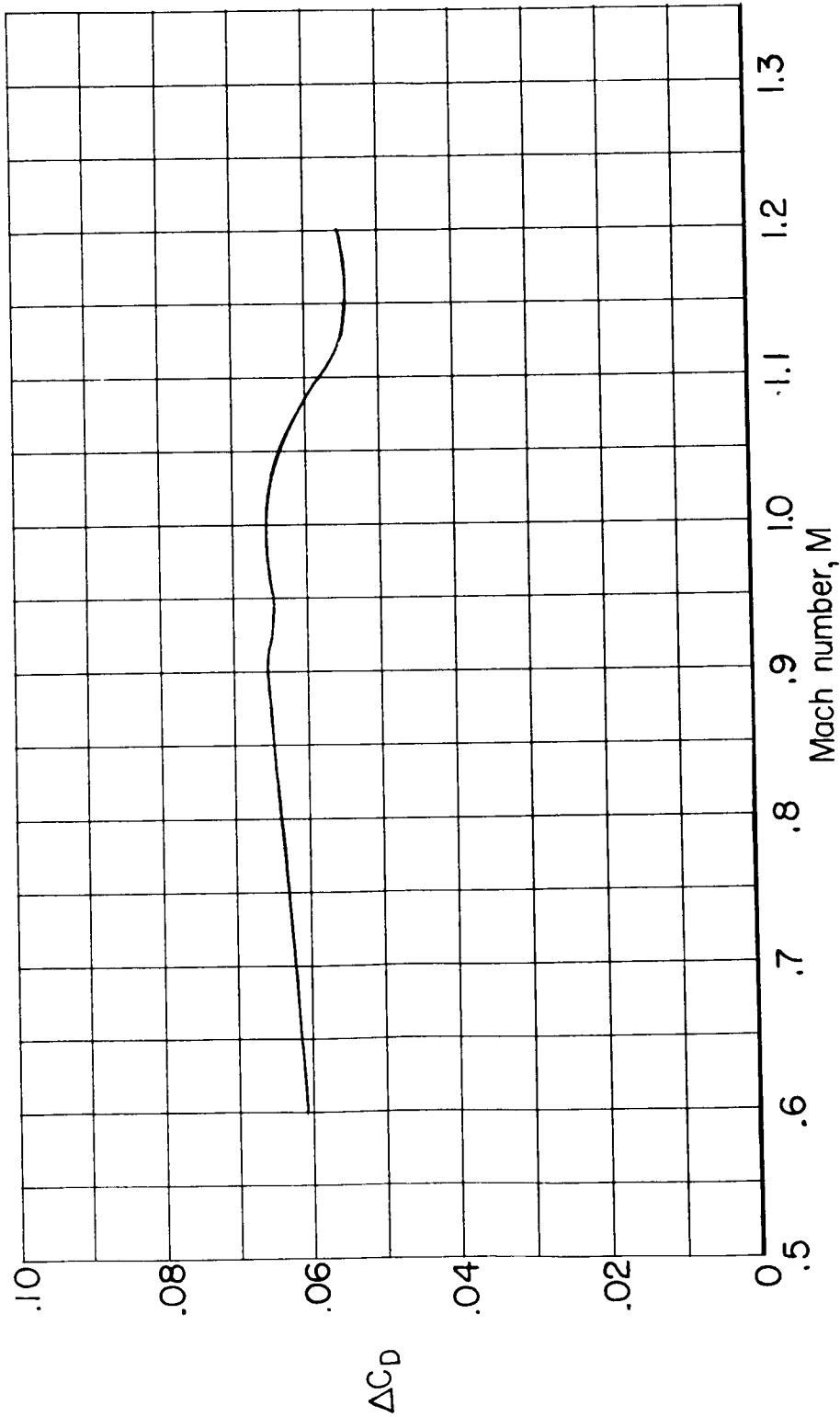


Figure 19.- Variation with Mach number of incremental drag coefficient due to speed brakes at zero lift. Configuration WB₂NH₀F₂V₁.